Available online at www.sciencedirect.com
ScienceDirect
Icarus 193 (2008) 1–19
ICARUS
www.elsevier.com/locate/icarus

# Predicting the Earth encounters of (99942) Apophis

Jon D. Giorgini [a,*], Lance A.M. Benner [a], Steven J. Ostro [a], Michael C. Nolan [b], Michael W. Busch [c]

[a] *Jet Propulsion Laboratory, California Institute of Technology, MS 301-150, 4800 Oak Grove Drive, Pasadena, CA 91109-8099, USA*
[b] *Arecibo Observatory, National Astronomy and Ionosphere Center, HC03 Box 53995, Arecibo, PR 00612, USA*
[c] *Division of Geological and Planetary Sciences, California Institute of Technology, Pasadena, CA 91125, USA*

Received 18 July 2007; revised 5 September 2007

Available online 9 October 2007

**Abstract**

Arecibo delay–Doppler measurements of (99942) Apophis in 2005 and 2006 resulted in a five standard-deviation trajectory correction to the optically predicted close approach distance to Earth in 2029. The radar measurements reduced the volume of the statistical uncertainty region entering the encounter to 7.3% of the pre-radar solution, but increased the trajectory uncertainty growth rate across the encounter by 800% due to the closer predicted approach to the Earth. A small estimated Earth impact probability remained for 2036. With standard-deviation plane-of-sky position uncertainties for 2007–2010 already less than 0.2 arcsec, the best near-term ground-based optical astrometry can only weakly affect the trajectory estimate. While the potential for impact in 2036 will likely be excluded in 2013 (if not 2011) using ground-based optical measurements, approximations within the Standard Dynamical Model (SDM) used to estimate and predict the trajectory from the current era are sufficient to obscure the difference between a predicted impact and a miss in 2036 by altering the dynamics leading into the 2029 encounter. Normal impact probability assessments based on the SDM become problematic without knowledge of the object's physical properties; impact could be excluded while the actual dynamics still permit it. Calibrated position uncertainty intervals are developed to compensate for this by characterizing the minimum and maximum effect of physical parameters on the trajectory. Uncertainty in accelerations related to solar radiation can cause between 82 and 4720 Earth-radii of trajectory change relative to the SDM by 2036. If an actionable hazard exists, alteration by 2–10% of Apophis' total absorption of solar radiation in 2018 could be sufficient to produce a six standard-deviation trajectory change by 2036 given physical characterization; even a 0.5% change could produce a trajectory shift of one Earth-radius by 2036 for all possible spin-poles and likely masses. Planetary ephemeris uncertainties are the next greatest source of systematic error, causing up to 23 Earth-radii of uncertainty. The SDM Earth point-mass assumption introduces an additional 2.9 Earth-radii of prediction error by 2036. Unmodeled asteroid perturbations produce as much as 2.3 Earth-radii of error. We find no future small-body encounters likely to yield an Apophis mass determination prior to 2029. However, asteroid (144898) 2004 VD17, itself having a statistical Earth impact in 2102, will probably encounter Apophis at 6.7 lunar distances in 2034, their uncertainty regions coming as close as 1.6 lunar distances near the center of both SDM probability distributions.


*Keywords:* Asteroids; Asteroids, dynamics; Radar observations; Near-Earth objects; Orbit determination

## 1. Introduction

Analyses of combined radar and optical measurements of (99942) Apophis (2004 MN4) have identified aspects warranting detailed assessment:

1) The object will pass the Earth's center at a distance of between $5.62R_\oplus$ and $6.30R_\oplus$ (where $R_\oplus = 6378.137$ km, one Earth equatorial radius in the WGS-84 system), on Friday, April 13, 2029 21:45 UTC. At this time, Apophis will be over the mid-Atlantic Ocean, north of Brazil, above 42.9° W, 29.0° N. An approach this close by an object this large (diameter $d \approx 270$ m) is thought to occur, on average, at intervals greater than ~800 years.
2) During the 2029 encounter, Apophis will be a 3rd-magnitude object visible to the unaided eye from Asia, Africa and Europe, even from large population centers with significant sky brightness. Having a visible disk 1.3 to 2.4 arcsec across, it should be resolvable by large ground-based optical telescopes and potentially imaged at meter-level res-

* Corresponding author.
*E-mail address:* jon.giorgini@jpl.nasa.gov (J.D. Giorgini).

0019-1035/$ – see front matter 
doi:10.1016/j.icarus.2007.09.012

olutions by radar at that time. The maximum plane-of-sky angular rate will be 50 arcseconds per second.

3) Apophis might experience spin-state alteration and geophysical deformation during the 2029 encounter due to Earth gravitational tides (Scheeres et al., 2005), depending on its internal structure.
4) A small Earth impact probability (IP) of 0.00224%, or 1 in 45,000 (1:45,000), on April 13, 2036 is currently estimated using standard dynamical models, despite optical and radar astrometry spanning more than one orbit period, including three sets of radar measurements separated by 18 months. Activists have called on NASA to place a transponder on the surface in support of a possible deflection mission (Schweickart, 2005).

In this paper, we present details of Arecibo radar observations of Apophis in 2005–2006 and their effect on our knowledge of its position in 2029 and 2036. We explore how such predictions are changed by six sources of systematic error normally not accounted for in asteroid orbit calculations. We then consider the progression of knowledge as future astrometric measurements are reported, presenting results that combine statistical simulations with parametrically determined systematic error bounds. This provides calibrated position uncertainty ranges for the 2036 encounter along with criteria for excluding the potential impact. While Apophis is very unlikely to be a hazard at that time, similar situations could occur in the future. Recognizing and propagating all sources of systematic and statistical uncertainties into a trajectory prediction can have significant implications for decisions relating to costly reconnaissance or mitigation missions.

The analysis described herein differs from an early study (Chesley, 2006) primarily in that it comprehensively assesses systematic errors and links them to the 2029 and 2036 encounter predictions with parametric intervals instead of impact probabilities based on assumed or synthesized normal distributions. Improved determinations of Apophis physical parameters are available and the astrometric data arc is extended in time by a factor of 1.8, including new measurements from the final radar opportunities prior to 2013.

## 2. Observational history

### 2.1. Initial characterization and astrometry

Apophis was first observed on June 19–20, 2004, using the 2.3-m Bok telescope at Kitt Peak (Tucker et al., 2004), designated as 2004 MN4, and then lost due to unfavorable weather. It was re-discovered on December 18, 2004, at Siding Spring Observatory (Garradd, 2004) and recognized as being the same object on December 20, 2004 (Smalley, 2004).

As new optical astrometric measurements were reported and corrected over the next several days, Earth impact probability estimates reached a maximum of 2.7% for April 13, 2029 (JPL Sentry on December 27, 2004; Chesley, 2006). This probability decreased to near zero later the same day, when pre-discovery astrometry derived from Spacewatch images recorded on March 15, 2004, were reported (Larsen and Descour, 2004). The measurements extended the data-arc by 96 days and eliminated the potential 2029 impact. However, there remained lower-probability impact risks in 2035, 2036, and 2037.

Near-infrared (0.8–2.5 micron) observations made by Binzel et al. (2007, Icarus, submitted for publication) place Apophis in the Sq spectral class and suggest its average geometric albedo is greater than 0.3, unless the surface is bare rock. Polarimetric measurements (Delbò et al., 2007) yield a geometric albedo ($p_v$) of $0.33 \pm 0.08$ (including estimated uncertainties in the slope–albedo relationship coefficients) and absolute visual magnitude ($H_v$) of $19.7 \pm 0.4$, from which the authors inferred an effective diameter ($d$) of $270 \pm 60$ m. Photometric lightcurves obtained by Behrend et al. (2005) indicate a rotation period of 30.4 h with a lightcurve amplitude of ∼0.9 magnitudes suggesting some elongation.

### 2.2. Radar observations

We observed Apophis from Arecibo in January 2005, August 2005, and May 2006. We obtained continuous wave (CW) Doppler echoes during each apparition (Fig. 1) and ranging echoes in January 2005 (Fig. 2). The echoes are weak due to the small size of the asteroid and its considerable distance at each opportunity (0.19–0.27 AU). Tables 1 and 2 summarize the observations and Apophis' disk-integrated radar properties.

#### 2.2.1. January 2005: Orbit debiasing

Based on impact probability estimates reported by JPL/Sentry and Pisa/NeoDys systems in December 2004, we scheduled Arecibo S-band (2380 MHz, 12.6 cm) radar observations for late January 2005, when Apophis entered Arecibo's declination window at a distance of 0.192 AU, the closest of the three radar opportunities. Using a tracking ephemeris initially based on the 506 optical measurements available over March 15, 2004 to January 24, 2005 (solution #50), we obtained three Doppler and two coarse-resolution range measurements (Benner et al., 2005) (Table 3).

The first echoes we acquired on January 27 were $4.8\sigma$ away from the frequency predicted by this optical-only solution (+2.8 Hz, or +176.4 mm s$^{-1}$ in radial velocity) (Fig. 1). The subsequent round-trip time (RTT) delay measured on January 29 was 4977.6 μs ($2.8\sigma$) less than predicted, or 746.1 km closer to Earth in range.

Incorporating these delay–Doppler measurements in a new weighted least-squares fit (solution #56) significantly corrected Apophis' orbit solution and revealed a previously undetected 1.4 arcsec systematic bias in the pre-discovery optical measurements (Giorgini et al., 2005a). It also moved the April 13, 2029 encounter 28,000 km ($4.4R_\oplus$) closer to the Earth. This was a $5\sigma$ encounter-trajectory correction (i.e., where the biased pre-radar optical solution assessment was 99.99995% certain it would not go), and moved the predicted point of closest approach inside Earth's geosynchronous satellite distance, although with a trajectory inclined at 40° with respect to the heavily populated equatorial satellite ring and passing outside that ring when crossing the equatorial plane.

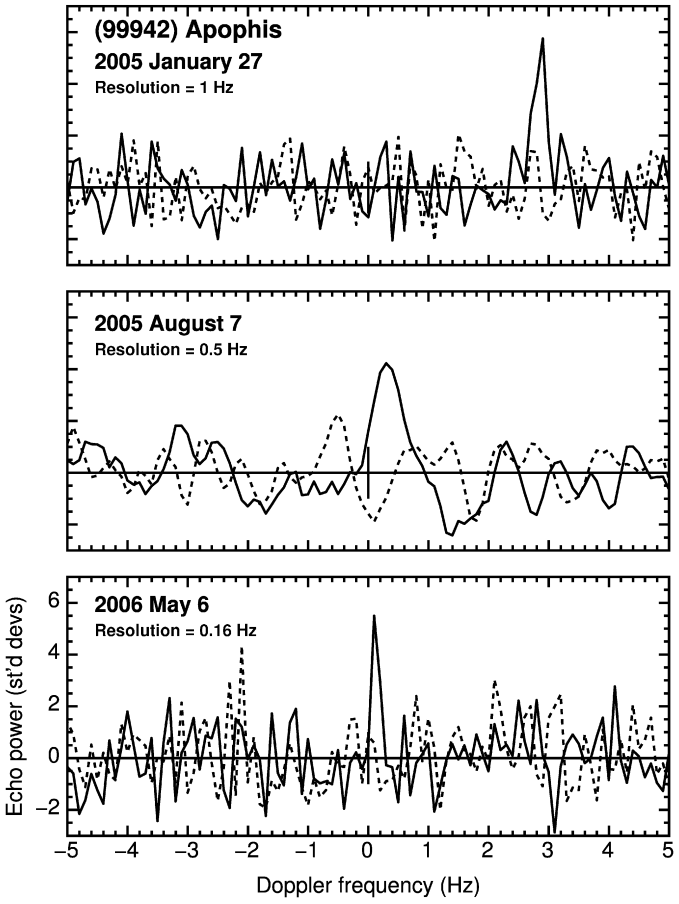


Fig. 1. Arecibo echo power spectra obtained during the three radar opportunities in 2005 and 2006. Solid and dashed lines show echo power in the opposite (OC) and same (SC) sense circular polarizations. Echo power in standard deviations of the noise is plotted as a function of Doppler frequency relative to the ephemeris predicted frequency for the asteroid's center of mass. The narrow bandwidth echo (typical of a slowly rotating asteroid) moved progressively closer to the plot center (i.e., zero offset) with each successive experiment as measurements from prior experiments were incorporated to improve the prediction ephemeris. Vertical scales are identical for each frame.

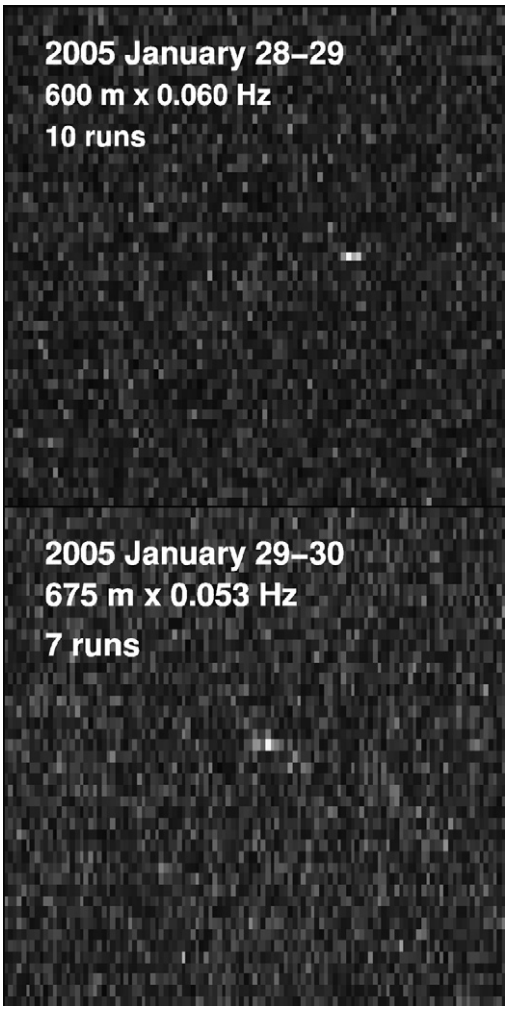


Fig. 2. Arecibo delay–Doppler summed images of Apophis in January 2005. Range increases from top to bottom and Doppler frequency from left to right with resolutions indicated. The images have the same Doppler and range extents of 6.0 Hz and 200 μs.

The problematic pre-discovery optical images were independently remeasured by two sources (Spahr and Smalley, 2005, personal communication). Each obtained new positions we found to be in agreement with each other and with the radar data. Post-fit residual mean and standard error of the six initially biased pre-discovery measurements are now $-0.01 \pm 0.058$ arcsec (R.A. $\times$ cos(Dec.)) and $-0.12 \pm 0.16$ arcsec (Dec.) with respect to the reference solution S142. The measurements are assigned standard error weights ($s_w$) equal to 1.0 arcsec in the fit.

The radar-corrected orbit (solution #56) obtained in January 2005 had better predictability (i.e., a smaller mapped covariance) up to 2029, but rapidly degraded thereafter. This was due to the new solution's deeper entry into the Earth's gravity field in 2029, an approach 45% closer than predicted prior to the radar observations (solution #50). The steeper gravity gradient differentially pulls on and elongates the statistical uncertainty space to a greater extent than the more distant uncorrected pre-radar encounter.

This deformation can be quantified using volume ratios of the "error ellipsoid" at times before and after an encounter. The covariance matrix $\boldsymbol{\Sigma}$ defines a region of space surrounding the nominal location in which the object may be located, bounded by a specified constant level of probability. It is computed using a matrix mapping operation

$$\boldsymbol{\Sigma} = \left(\boldsymbol{M}\boldsymbol{R}^{-1}\right)\left(\boldsymbol{M}\boldsymbol{R}^{-1}\right)^{\mathrm{T}}, \tag{1}$$

where $\boldsymbol{M}$ is a state-transition matrix whose elements are composed of the numerically integrated variational partial derivatives $\partial \boldsymbol{x}/\partial \boldsymbol{x}_0$, which relate the initial position and velocity state vector $\boldsymbol{x}_0$ at time $\tau_0$ to the state vector $\boldsymbol{x}$ at another time, $\tau$. Higher order terms in the derivatives are excluded, linearizing the operation. Given matrix $\boldsymbol{R}^{-1}$, the upper-triangularized square-root of the covariance matrix at the solution epoch $\tau_0$, $\boldsymbol{\Sigma}$ is the mapped covariance matrix at time $\tau$. The eigenvectors and eigenvalues of this matrix define the axes and size of a three-dimensional error ellipsoid (i.e., the "uncertainty region").

Table 1
Apophis radar observation log summary

| Date | R.A. (deg) | Dec. (deg) | Dist. (AU) | Setup | Code | Soln | $TX_{off}$ (Hz) | Ptx (kW) | Runs | UTC start | UTC stop | Echo? | Notes |
|---|---|---|---|---|---|---|---|---|---|---|---|---|---|
| 2005 Jan 27–28 | 60 | +01 | 0.189 | CW | | 50 | +200 | 779 | 4 | 232448 | 234646 | Yes | |
| | | | | 4.0 μs | 8191 | 52 | +2 | 760 | 7 | 235229 | 003318 | No | |
| 2005 Jan 28–29 | 61 | +02 | 0.192 | 4.0 μs | 8191 | 52 | +2 | 782 | 10 | 232139 | 002229 | Yes | |
| | | | | 4.0 μs | 1023 | 52 | +2 | 782 | 2 | 002853 | 003824 | No | |
| 2005 Jan 29–30 | 62 | +02 | 0.196 | 4.5 μs | 8191 | 54 | +2 | 740 | 7 | 235139 | 003359 | Yes | |
| 2005 Aug 07 | 146 | +23 | 0.268 | CW | | 106 | +200 | 400 | 18 | 154855 | 182524 | Yes | |
| 2005 Aug 08 | 145 | +23 | 0.268 | 4.0 μs | 8191 | 106 | +2 | 430 | 18 | 154047 | 181659 | No | |
| 2006 May 06 | 348 | +02 | 0.260 | CW | | 130 | +200 | 812 | 9 | 121151 | 132523 | Yes | |
| 2006 May 07 | 349 | +03 | 0.264 | 4.0 μs | 8191 | 130 | +2 | 813 | 6 | 115925 | 123005 | No | Turbine problem |
| | | | | 4.0 μs | 8191 | 130 | +2 | 811 | 2 | 131825 | 133129 | No | |
| 2006 May 08 | 351 | +03 | 0.269 | 4.0 μs | 8191 | 130 | +2 | 762 | 1 | 124908 | 125326 | No | Turbine and klystron problem |
| 2006 May 09 | 352 | +04 | 0.273 | 4.0 μs | 8191 | 130 | +2 | 800 | 10 | 115707 | 132326 | No | Turbine problem |

*Notes*. "R.A.," "Dec.," and "Dist." are the right ascension, declination, and geocentric distance. "Soln" is the orbit solution. "$TX_{off}$" is the transmitter offset. "Ptx" is the transmitter power. "Runs" refers to the number of transmit-receive cycles.

Table 2
Apophis radar properties

| Date | OC SNR | OC×sec ($km^2$) | SC/OC | Resolution (Hz) |
|---|---|---|---|---|
| 2005 Jan 27 | 7.2 | 0.015 | $0.0 \pm 0.10$ | 0.1 |
| 2005 Aug 07 | 4.3 | 0.029 | $0.0 \pm 0.15$ | 0.5 |
| 2006 May 06 | 5.5 | 0.013 | $0.29 \pm 0.15$ | 0.16 |

*Notes*. "OC SNR" is the optimally-filtered SNR for the opposite-sense circular polarization ("OC") echo (relative to the transmitted signal). "SC" denotes same-sense circular polarization echoes. "OC×sec" is the OC radar cross-section; uncertainties are dominated by systematic pointing and calibration errors. The cross-sections and circular polarization ratio SC/OC were estimated using the frequency resolutions shown. For SC/OC, a measure of near-surface complexity at the 12.6 cm wavelength (and a crude estimate of the fraction of the surface area covered by wavelength-sized rocks), systematic effects cancel and most remaining statistical errors propagate from receiver thermal noise. Apophis thus appears to be smoother than the average radar-detected NEA (at 13 cm scales), the average SC/OC being $0.33 \pm 0.23$ (RMS), with a median of 0.25. See Ostro et al. (2002) for discussion of asteroid radar properties.

Without the delay–Doppler measurements, the more distant geocentric encounter predicted prior to the radar experiment ($10.2 R_\oplus$) had an error ellipsoid volume ratio of 25.5 (computed at the same times, 3 days after/before). The radar-corrected orbit solution had a much closer predicted encounter ($5.6 \pm 1.6 R_\oplus$) and a larger ±3 day volume ratio of 201. While delay and Doppler measurements reduced the volume of the predicted uncertainty region going into the 2029 encounter by 93%, reduction after the encounter was only 43%, with an 800% increase in the rate of uncertainty growth across the encounter, due to the much closer predicted Earth approach.

With the orbit and measurement statistics corrected, we used a Monte Carlo method to examine uncertainties after 2029, when the linearized Eq. (1) no longer has acceptable accuracy. The full six-dimensional position-velocity state uncertainty region at the solution epoch was sampled 10,000 times, approximately characterizing the Gaussian uncertainty region with 99.7% confidence limits ($\pm 3\sigma$). Each trajectory was then separately propagated from those initial conditions using the complete non-linear parameterized post-Newtonian $n$-body equations of motion (Moyer, 1971).

This $\pm 3\sigma$ uncertainty region in 2036, derived from solution #106 in July of 2005, wrapped around the Sun through ∼152° of heliocentric longitude (Fig. 3), a significant reduction from 260° prior to the radar experiment. Position uncertainties increased most rapidly in the along-track direction of orbital motion. Although it wasn't certain on which side of the Sun Apophis would be in 2036, the new center of the probability region was only two lunar distances from Earth on April 13.375,

Table 3
Apophis radar astrometry

| Date YYYY MM DD | UTC HH:MM:SS | Measurement | Unit | Type | $s_w$ (Hz or μs) | Residual (Hz or μs) |
|---|---|---|---|---|---|---|
| 2005 01 27 | 23:31:00 | −100849.1434 | Hz | Doppler | 0.25 | −0.016 |
| 2005 01 29 | 00:00:00 | −102512.9059 | Hz | Doppler | 0.25 | 0.053 |
| 2005 01 29 | 00:00:00 | 192.0285071 | s | RTT | 4.0 | 0.700 |
| 2005 01 30 | 00:18:00 | −103799.8178 | Hz | Doppler | 0.15 | 0.097 |
| 2005 01 30 | 00:18:00 | 195.8081708 | s | RTT | 4.5 | −0.598 |
| 2005 08 07 | 17:07:00 | 8186.8 | Hz | Doppler | 0.2 | −0.094 |
| 2006 05 06 | 12:49:00 | −118256.8 | Hz | Doppler | 0.1 | 0.054 |

*Notes*. Apophis radar astrometry. Entries report the measured round-trip time (delay) and Doppler frequency for echoes from Apophis' estimated center-of-mass received at the indicated UTC epoch. The reference point for Arecibo is the center-of-curvature of the 305 m antenna. The assigned standard errors ($s_w$) reflect imaging and frequency resolution and echo strength. 1 μs of round-trip delay corresponds to ∼150 m in range; 1 Hz in Doppler corresponds to ∼63 mm $s^{-1}$ in radial velocity at the 2380 MHz Arecibo S-band transmitter frequency. Residuals are the observed minus computed (O − C) difference between measurement and the prediction of orbit solution S142.

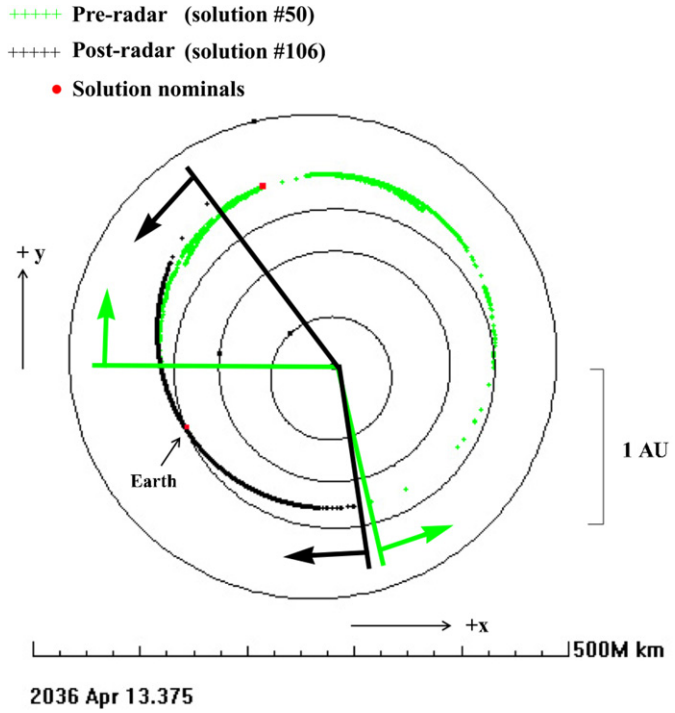


Fig. 3. SDM Monte Carlo results projected onto the J2000 ecliptic plane as viewed from ecliptic north. The Sun is at the center. The orbits of the inner four planets are marked with black ellipses. 10,000 statistically possible orbits were sampled from both solution #50 (i.e., before the January 2005 radar astrometry, in green) and solution #106 (i.e., after the first radar track, in black) uncertainty regions, then propagated individually from 2005 to the 2036 encounter using the non-linear SDM. Red squares mark the nominal (highest probably) location of Apophis for each solution. Radial lines from the Sun mark the extent of each $\sim 3\sigma$ Monte Carlo uncertainty region. Comparison of the regions reveals Arecibo measurements correcting an optical data bias and reducing uncertainties, but placing the new nominal solution near the Earth in 2036, producing a small impact probability under the SDM.

2036, where one lunar distance (LD) equals 384,400 km. With impacting solutions drawing from the $0.1\sigma$ region of the distribution, the impact probability estimate was $\sim 10^{-4}$.

*2.2.2. August 2005: Uncertainty reduction*

Arecibo radar observations of Apophis on August 7, 2005 produced a weak CW detection (Fig. 1) and a single Doppler measurement from a distance of 0.268 AU (Giorgini et al., 2005b); a correction of $+0.3 \pm 0.2$ Hz ($+18.9 \pm 12.6$ mm s$^{-1}$) relative to the pre-experiment prediction of solution #106 (which was based on 755 optical measurements made between March 15, 2004 and July 11, 2005, and the 2 delays and 3 Dopplers from January). The observations were hampered by the loss of one klystron that limited the transmitter to one-half of its normal power. The radar cross section was nearly double that obtained in January, which could be explained by a more broadside orientation in August or, given such a low SNR, by uncalibrated error sources.

Including the new Doppler correction in a new orbit estimate (solution #108) increased the nominal 2029 Earth close-approach distance from $5.77 \pm 0.20 R_\oplus$ to $5.86 \pm 0.12 R_\oplus$ and reduced the along-track position uncertainty at closest-approach by 61%, from $\pm 2031$ to $\pm 787$ km ($1\sigma$). The volume of the three-dimensional error ellipsoid entering the encounter decreased 76%.

The new Doppler measurement eliminated a statistically small Earth impact possibility in 2035. For the 2036 encounter, the new Doppler measurement increased from 0.005 to 0.14 AU the predicted nominal Earth close approach, but did not greatly change the impact probability because the uncertainty region, while smaller, remained centered only 0.14 AU from Earth.

*2.2.3. May 2006: Uncertainty reduction*

We observed Apophis from Arecibo a third time, during May 6–8, 2006, when the asteroid was 0.260 AU from Earth, obtaining CW echoes with a SNR of 5.5 (Fig. 1) (Benner et al., 2006). We measured a Doppler correction of $+0.1 \pm 0.1$ Hz ($+6 \pm 6$ mm s$^{-1}$) relative to pre-experiment solution #130, which was a fit to 779 optical observations between March 15, 2004 and March 26, 2006, and 2 delay and 4 Doppler measurements.

Incorporating the new Doppler in solution #140 increased the predicted nominal miss-distance in 2029 by 600 km, from $5.86 \pm 0.11 R_\oplus$ to $5.96 \pm 0.09 R_\oplus$, and reduced the along-track position uncertainty at closest approach from $\pm 753$ to $\pm 588$ km ($1\sigma$). The volume of the uncertainty region predicted for 2029 decreased 23%. The predicted nominal close-approach distance in 2036 increased from 0.168 to 0.313 AU, with the Earth encounter moving from a point at $1.2\sigma$ (IP = 1:6,200) to a point at $2.1\sigma$ (IP = 1:24,000) in the probability distribution.

Inclusion of several subsequent optical measurements, weighted at 0.5 and 0.3 arcsec, extended the data-arc more than two months to August 16, 2006, and produced the current best estimate study solution "S142," which has a nominal Earth-centered approach of $5.96 \pm 0.08 R_\oplus$ in 2029. The orbit solution and covariance were developed in a standard way according to the principles discussed in Appendix A. Considering systematic error sources not included in the formal covariance (but subsequently described herein), the minimum geocentric encounter distance in 2029 will be within the interval $[5.62, 6.30] R_\oplus$.

The highest probability outcome predicted with standard dynamical models for April 13 (Easter Sunday) of 2036 is a distant 0.34 AU passage. However, the S142 set of statistically possible orbits ($\pm 3\sigma$) extends through $\sim 72°$ of heliocentric longitude at that time, intersecting the Earth's orbit $-2.4\sigma$ from the center of the probability distribution (Fig. 4). An impact probability of 1:45,000 therefore remains, given standard dynamical models. Solution "S142" orbit and goodness-of-fit parameters are collected in Table 4 as the reference orbit for the remainder of this paper. Figs. 5a–5b show Apophis optical residuals for S142.

## 3. Predictability

### *3.1. Trajectory prediction uncertainty*

*3.1.1. Planetary encounter predictability*

The accuracy of a trajectory prediction depends on the fraction of the orbit sampled by astrometry, the accuracy and precision of those measurements, the interval between the time of measurement and time of prediction, and the dynamics of the

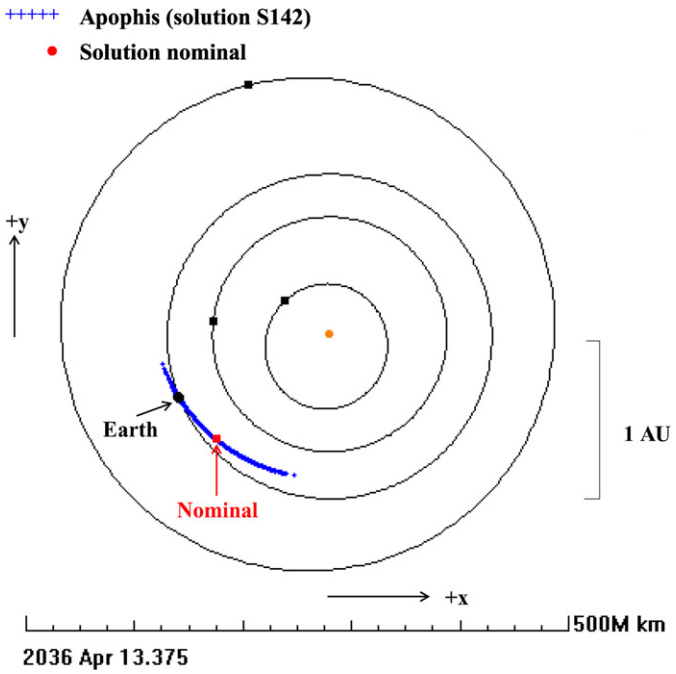


Fig. 4. Current Apophis SDM reference solution S142 Monte Carlo results projected into the J2000 ecliptic plane as viewed from ecliptic north. Earth impact currently occurs at $\sim -2.4\sigma$ within the S142 probability distribution. If there were no SDM or measurement biases, the measurement uncertainty region would shrink around the current nominal position, as new measurements accumulated, until the Earth no longer encountered the region, thereby excluding impact.

Table 4
Apophis reference orbit solution S142

| Osculating element | Value | $\sigma_u$ |
|---|---|---|
| Eccentricity ($e$) | 0.1910573105795565 | ±0.0000000297 |
| Perihelion distance ($q$) | 0.7460599319224038 | ±0.0000000339 AU |
| Perihelion date ($T_p$) | 2453924.3091729818 | ±0.0000076340 d (JD) |
| Longitude of ascending node ($\Omega$) | 204.45996801109067 | ±0.0000425720 deg |
| Argument of perihelion ($\omega$) | 126.39643948747843 | ±0.0000422150 deg |
| Inclination ($i$) | 3.33132242244163 | ±0.0000007966 deg |
| Semimajor axis ($a$) | 0.9222654975186300 | ±0.0000000096 AU |
| Orbit period, sidereal ($P$) | 323.5060220661519 | ±0.00000504 d |
| Mean anomaly ($M$) | 61.41677858002747 | ±0.0000010854 deg |

*Notes*. Estimated heliocentric J2000 ecliptic osculating elements with unbiased standard deviations ($\sigma_u$) at the solution epoch 2006-September-1.0 (JD 2453979.5) Coordinate Time (where CT is the independent variable in the relativistic dynamical equations of motion). Estimated using two delay and five Doppler measurements (Table 3) combined with 792 optical measurements (2004-March-15 to 2006-August-17). Post-fit R.A. residual mean is 0.004″, Dec. mean is 0.022″, with normalized RMS ($\text{RMS}_n$; the quadratic mean of all optical measurements divided by their individual assigned uncertainties) of 0.407. Delay (mean, $\text{RMS}_n$) is (0.051 μs, 0.155). Doppler (mean, $\text{RMS}_n$) is (0.019 Hz, 0.441). Combined optical and radar $\text{RMS}_n$ is 0.407. The solution was estimated in the dynamical system defined by the JPL planetary ephemeris DE405, a quasar-based radio frame generally within 0.01 arcsec of the optical FK5/J2000 frame. Angular elements are expressed with respect to the J2000 ecliptic plane. Prior solutions mentioned in the text are available from the author or JPL.

model used to propagate the non-linear equations of motion. The Standard Dynamical Model (the SDM), used for all routine asteroid solutions and propagations, includes $n$-body relativistic gravitational forces caused by the Sun, planets, Moon, Ceres, Pallas, and Vesta.

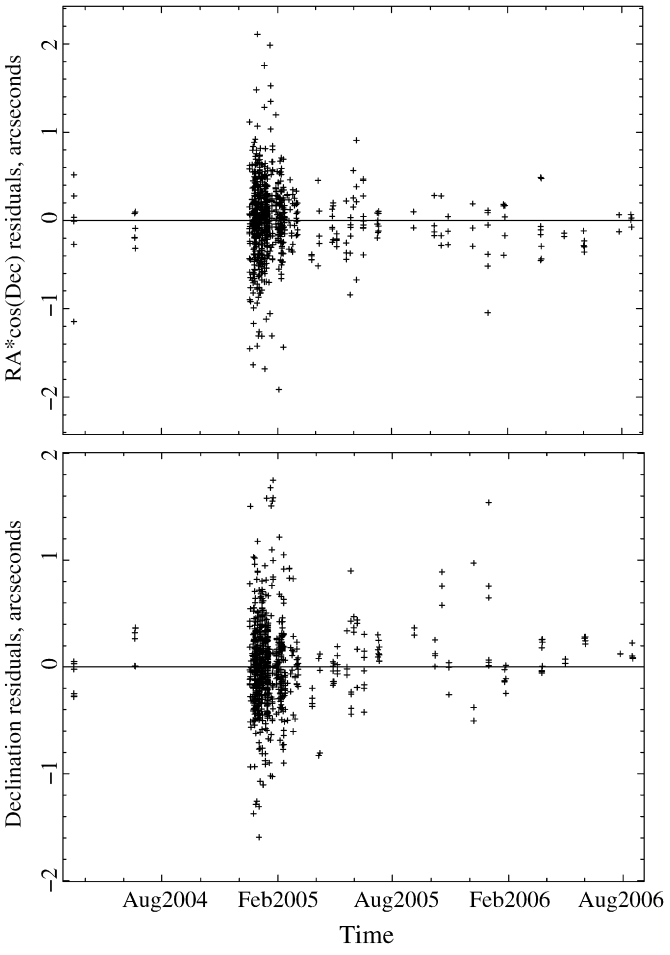


Fig. 5. (a) Apophis SDM solution S142 post-fit R.A. × cos(Dec.) residuals: the observed minus computed difference between predicted SDM plane-of-sky position and reported measurements. (b) Apophis SDM solution S142 post-fit Dec. residuals. See Table 4 for the orbit solution these residuals are with respect to (along with summarizing statistics) and Table 3 for the delay–Doppler radar residuals.

Orbit solution uncertainties normally increase with time from the epoch of the measurements (except for well-determined orbits in gravitational resonances; see Giorgini et al., 2002, for example) and are further amplified during close planetary encounters. To identify bounding limits of deterministic prediction, Apophis reference solution S142 was numerically integrated backward and forward in time from the September 1, 2006 solution epoch.

We identified Earth encounters closer than 0.1 AU, where the linearized $3\sigma$ uncertainty in encounter time was less than 10 days and the $3\sigma$ uncertainty in approach distance was less than 0.1 AU. Encounters having uncertainties greater than one of these criteria usually correspond to a planetary approach (verifiable using a non-linear Monte-Carlo simulation) that disrupts the uncertainty region such that a linearized covariance mapping is no longer valid (Ostro and Giorgini, 2004).

The specific interval satisfying these criteria for Apophis is 1889 to 2029 (Table 5). For solutions based on the S142 dataset,

Table 5
Planetary close approaches

| Date (CT) | Body | CA_Dist (AU) | MinDist (AU) | MaxDist (AU) | $V_{rel}$ (km s$^{-1}$) | TCA_3$\sigma$ (min) |
|---|---|---|---|---|---|---|
| 1869 Apr 09.26044 | Venus | 0.074971 | 0.065571 | 0.094903 | 4.667 | 2921.8 |
| 1886 Dec 31.95830 | Venus | 0.091663 | 0.084564 | 0.107005 | 5.460 | 1550.8 |
| 1889 Dec 16.67897 | Earth | 0.049299 | 0.049081 | 0.049784 | 5.566 | 174.47 |
| 1907 Apr 13.14345 | Earth | 0.027612 | 0.024830 | 0.030474 | 5.123 | 383.44 |
| 1922 Oct 16.91555 | Venus | 0.075562 | 0.074549 | 0.076640 | 4.276 | 99.31 |
| 1922 Dec 19.14874 | Earth | 0.114676 | 0.112793 | 0.116557 | 8.956 | 77.87 |
| 1924 Apr 13.25917 | Earth | 0.108630 | 0.106480 | 0.110770 | 9.092 | 68.21 |
| 1932 Mar 08.30531 | Earth | 0.114169 | 0.113545 | 0.114797 | 4.550 | 1370.8 |
| 1939 Dec 18.70630 | Earth | 0.060007 | 0.059577 | 0.060450 | 4.750 | 69.34 |
| 1949 Apr 14.47917 | Earth | 0.027916 | 0.027793 | 0.028039 | 6.689 | 0.16 |
| 1950 Jun 26.17919 | Venus | 0.091335 | 0.091231 | 0.091438 | 6.619 | 6.67 |
| 1957 Apr 01.11402 | Earth | 0.075453 | 0.075290 | 0.075616 | 4.281 | 111.39 |
| 1968 Mar 20.09653 | Venus | 0.084186 | 0.084154 | 0.084217 | 4.277 | 16.11 |
| 1968 Apr 25.67812 | Venus | 0.085869 | 0.085793 | 0.085945 | 3.265 | 0.63 |
| 1972 Dec 24.48247 | Earth | 0.079213 | 0.079140 | 0.079286 | 4.057 | 36.98 |
| 1980 Dec 18.07855 | Earth | 0.072143 | 0.072095 | 0.072191 | 7.351 | 2.89 |
| 1990 Apr 14.86420 | Earth | 0.032939 | 0.032909 | 0.032969 | 6.845 | 0.07 |
| 1994 Jan 21.51069 | Venus | 0.082654 | 0.082652 | 0.082657 | 4.045 | 2.20 |
| 1994 Feb 26.49992 | Venus | 0.082881 | 0.082873 | 0.082889 | 3.381 | 0.63 |
| 1998 Apr 14.82361 | Earth | 0.024385 | 0.024381 | 0.024390 | 6.585 | 0.07 |
| 2004 Dec 21.39226 | Earth | 0.096384 | 0.096384 | 0.096384 | 8.226 | 0.04 |
| 2013 Jan 09.48850 | Earth | 0.096662 | 0.096659 | 0.096664 | 4.087 | 3.68 |
| 2016 Apr 24.11791 | Venus | 0.078241 | 0.078237 | 0.078245 | 6.089 | 0.35 |
| 2021 Mar 06.05209 | Earth | 0.112651 | 0.112648 | 0.112654 | 4.585 | 7.90 |
| 2029 Apr 13.90711 | Earth | 0.000254 | 0.000244 | 0.000265 | 7.422 | 0.66 |
| 2029 Apr 14.60586 | Moon | 0.000641 | 0.000616 | 0.000668 | 6.396 | 7.77 |

*Notes*. Encounter minima less than 0.12 AU are shown for that time-span in which the SDM 3$\sigma$ uncertainty in Earth encounter distance predicted by S142 is less than $\pm$0.1 AU, or time-of-encounter 3$\sigma$ uncertainty is less than $\pm$10 days, whichever occurs first. "CA_Dist" is the nominal encounter distance (to center of "Body"), "MinDist" and "MaxDist" are the 3$\sigma$ uncertainties in "CA_Dist" at the nominal time shown. "$V_{rel}$" is the relative velocity. "TCA_3$\sigma$" is the 3$\sigma$ uncertainty in the time of closest approach.

Earth encounters outside this time-span require non-linear parametric or statistical approaches.

### *3.1.2. Physical parameter uncertainties*

For asteroids having multiple intervening planetary encounters, significant prediction error can result when using the SDM because of mismodeled thermal radiation acceleration, asteroid perturbations, solar radiation pressure, and planetary mass uncertainties, among other issues (Giorgini et al., 2002). Such influences are not normally included in trajectory analyses, being insignificantly small relative to measurement uncertainties, a function of unmeasured object physical parameters, or computationally impractical.

These factors accumulate most error in the along-track direction in part since perturbations or estimation errors in four of six orbital elements ($a$, $e$, $\omega$, $T_p$; see Table 4 for definitions) directly contribute components in the along-track direction, having non-zero derivatives with respect to that coordinate. Therefore, knowledge of the position along the orbit path (i.e., timing) tends to degrade more quickly than knowledge of other position components.

While the rate of accumulated error will differ for different unmodeled forces, it can be problematic to attribute a measured offset from prediction at one instant (or even multiple instants) to only one factor or another without an analysis usually precluded by a lack of physical knowledge of the body or the complete dynamics.

With the orbit of Apophis increasingly well characterized and the potential impact in 2036 contingent on small details of the 2029 encounter (requiring passage through a region of space comparable in size to the asteroid), we extend Giorgini et al. (2005c) by examining the influence of such dynamical effects. Each was found capable of altering Apophis' impact-trajectory prediction in 2036 by changing the location and extent of the set of encounter states in 2029 that allow for a later impact.

These additional factors can be classified in two groups. Group 1 includes factors with small effects comparable to integration error (such as Earth's non-uniform mass distribution and planetary ephemeris errors), and those (such as asteroid perturbations) that are unlikely to be conclusively measured prior to 2029, since astrometric measurements have little sensitivity to them. Group 2 includes factors that might be observed and estimated from measurement prior to 2029, such as thermal radiation acceleration, which produces the "Yarkovsky effect," and solar radiation pressure.

*Group 1 parameters* The slight, cumulative mismodeling of Group 1 parameters is normally aliased into the estimated orbital elements. A question in this situation is: what error can result for a trajectory prediction based on an initial state estimate known to be systematically biased? This is relevant because mission studies must normally begin by propagating such biased estimates, lacking an alternative.

To address this question, we fit the measurement data using the SDM and weighted least-squares to obtain a position-velocity state estimate. We then augmented the SDM for times after the end of the fit data-arc (i.e., beginning at the September 1, 2006 solution covariance epoch) by incorporating additional models whose parameters were assigned possible values, as described below. We then propagated a trajectory from the estimated state vector using this augmented model and compared the result to a propagation of the same initial state based on the SDM. *We refer to this approach as the fit-discontinuous model.* We considered two trajectories in this way: the nominal trajectory and an off-nominal ($-2.4\sigma$) trajectory that impacts in 2036 under the SDM (i.e., the impacting trajectory $Z$-score is $-2.4$).

The trajectory difference (the Euclidean metric) for the fit-discontinuous model indicates how the perturbation, cumulatively acting on an initially biased state uninformed of the dynamical effect, will cause a deviation in prediction relative to a situation where the particular perturbation is zero. Since the initial state estimate is biased (the particular perturbation probably not being zero), the resulting difference will misstate the change caused by the perturbing force alone, but does show what error will occur in typical trajectory predictions.

The fit-discontinuous case is similar to the normal situation for asteroid orbit solutions; the SDM is used to fit the measurements and estimate a state at an instant. The true state subsequently continues to evolve according to actual dynamics. In practice, the prediction error on any given future date tends to decrease as the data-arc lengthens towards that date; mismodeling within the lengthening data-arc is aliased into the state estimate to an increasing level, potentially producing slightly larger measurement fit residuals.

*Group 2 parameters* For thermal radiation and solar radiation pressure forces, a question is: what is the effect of the perturbation relative to the SDM? This is relevant since it may be possible to eventually observe and estimate the effect along with the orbital element state.

To address this question, we incorporated an extended dynamical model into a weighted least-squares estimate of the orbital elements. Parameters such as diameter or spin vector were assigned test values but not estimated. The new state elements, now estimated to be consistent with the extended dynamical model, initialized a numerical integration with that same extended model. We then compared the resulting trajectory to the prediction of the SDM. *We refer to this approach as the fit-continuous model.*

The trajectory difference for the fit-continuous model indicates how the perturbation will affect both the state estimate and the motion of the object relative to the standard model. This can provide insight into when it might be possible to detect the perturbation as the solution is updated with new astrometric measurements.

The fit-continuous and fit-discontinuous models let us distinguish between the consequences of a perturbation and the prediction error of an incomplete dynamical model.

*Numerical integration* We used a variable order, variable step-size, Adams–Krogh method with error monitoring and control logic to numerically integrate the second-order ordinary differential equations of motion (Krogh, 1968, 1974). The algorithm is used for JPL spacecraft navigation, asteroid radar tracking, gravity field analyses, and planetary ephemeris development. The predicted trajectories are repeatedly tested against measurement as part of the orbit determination process. Examples include successful prediction of the NEAR spacecraft's Earth to Eros range measurements at the 2-m level over a one-year integration (once the primary dynamical models were complete), and recovery of the position of minor planet 1862 Apollo to within 1-km after integrating back 100 years (from 1998), then forward again (200 years in total, with 24 planetary encounters less than 0.1 AU).

*3.1.2.1. Planetary ephemeris uncertainties* A planetary ephemeris specifies most dynamical parameters for orbital motion within the Solar System, defining the scale, masses, position, and velocity of the perturbing planets, Moon and Sun, relative to the Solar System barycenter. We used JPL's DE405 solution (Standish, 1998), a least-squares $n$-body fit to spacecraft, radar, VLBI, lunar-laser ranging, and telescopic measurements made over several centuries up to 1998.

DE405 has its own error covariance matrix for estimated parameters such as planetary states and masses. This statistical error model, although small in the present era, is uncalibrated in that it does not reflect unmodeled error sources aliased into the solution.

To better quantify such error, we used the transitional DE414 solution (Standish, 2006) for comparison. DE414 is a recent Solar-System solution based on ten additional years of spacecraft tracking, telescopic CCD data, and improved dynamical models. The difference between DE405 and DE414 provides a more calibrated indicator of the true errors than DE405's formal covariance matrix and an upper bound on errors in Apophis prediction due to the planetary ephemeris.

Results for the fit-discontinuous impacting case show that a difference of 1.2 km in Apophis location accumulated by April 13, 2029 grows to 28,600 km ($4.5R_\oplus$) by April 13, 2036 (Fig. 6, Table 6a). When DE414 is used to refit the data for the fit-continuous model, the difference is 3 km by 2029 and 148,000 km ($23R_\oplus$) by 2036. This occurs primarily because DE414 has an estimated perturbing Earth mass $1.36 \times 10^{-5}\%$ greater than DE405 from a location displaced $\sim$1 km in heliocentric coordinates during the 2004 Apophis Earth encounter. This changes the dynamics of the 2004 encounter for the solution and subsequent perturbations.

Future use of DE414 or follow-on planetary ephemerides will produce predictions with less error. However, the uncertainty introduced by DE405 is currently such that, even if the position of Apophis is expressed perfectly by S142, up to $23R_\oplus$ of prediction error could accumulate by the time of the 2036 encounter primarily as a consequence of planetary ephemeris error being amplified by the unusually close Earth encounter in 2029.

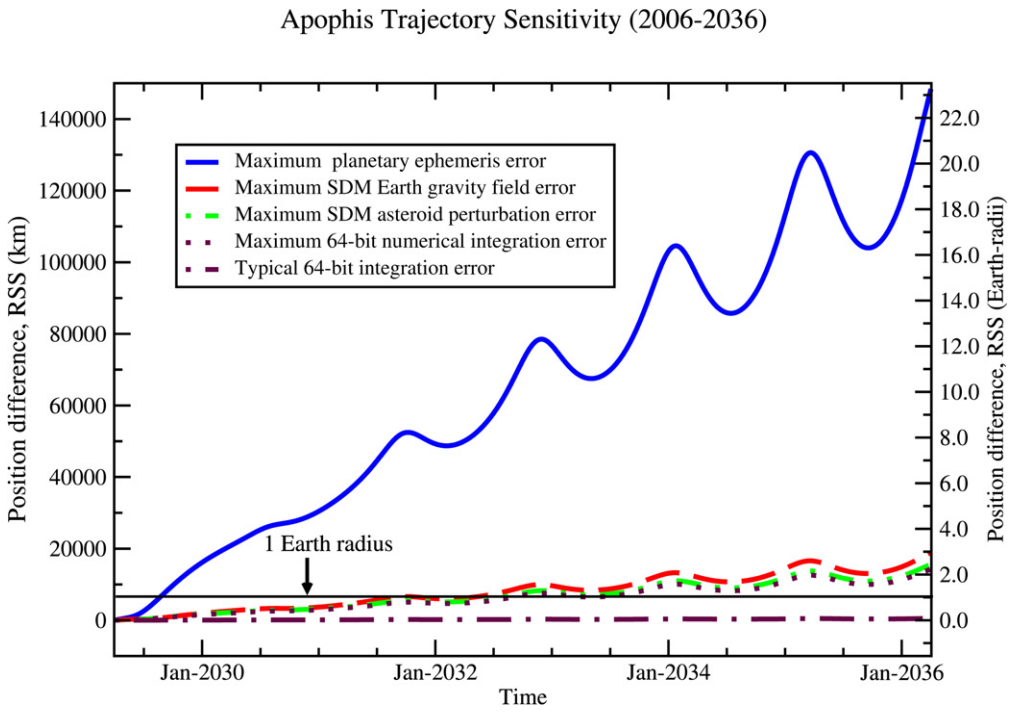


Fig. 6. Maximum trajectory prediction error accumulated between 2006 and 2036 as a result of unmodeled asteroid perturbations, planetary ephemeris error, and Earth point-mass assumptions. Maximum and typical 64-bit integration error is shown (see also Table 6a). Only results after the 2029 Earth encounter are plotted.

*3.1.2.2. Asteroid–asteroid perturbations* Although our orbit solutions include gravitational perturbations due to the three largest objects in the main belt (Ceres, Pallas, and Vesta, having ∼65% of the main belt's total mass), any object may be influenced more significantly by encounters with other objects. Encounters that are well-observed, close, and at low relative velocity might also permit estimation of an asteroid's mass.

Close approaches by Apophis to other objects were checked by numerically integrating 373,000 known asteroids between 2004 and 2036, estimating their individual gravitational influence by 2036 on Apophis using the method described in Giorgini et al. (2002). The top four perturbing objects for Apophis during 2004–2036 are Ceres, Vesta, Pallas, and Hygiea, accounting for 68.3% of the total detected perturbation, with Juno and Psyche the next most significant grouping (Table 7). The closest predictable encounter will be with 2001 GQ2 at 0.63 lunar distances in January 2027. The largest asteroid Apophis will encounter is the 3–9 km diameter object (85713) 1998 SS49 in June 2020, at 1.55 LD. Of the 50 closest encounters, the one with the smallest relative velocity (5.5 km $s^{-1}$) having an orbit sufficiently well-determined to predict an encounter is 2000 EA14. It will pass at 1.89 LD in May 2009. No future small-body encounters likely to yield an Apophis mass determination prior to 2029 were found within the set of currently known objects.

We examined the combined influence of the 128 top-ranked perturbers, which account for 93% of the total detected perturbation, using the fit-discontinuous and fit-continuous models. The impact-trajectory offset for the fit-discontinuous model remains less than 400 m until the 2029 encounter, after which it grows rapidly, reaching 14,700 km on April 13, 2036 (Fig. 6). Repeating the propagation with the top 64, 32, 16 and 8 perturbers produced offsets of 13,900, 12,600, 7900, and 3000 km, indicating little sensitivity to more than the first 32 perturbers. Results for the S142 nominal orbit are similar (Table 6a). When additional perturbing asteroids are included in the dynamics of a new least-squares solution (the fit-continuous case), the displacement amounts to 100–200 m by the 2029 encounter but is comparable to the radius of the Earth by 2036 (Table 6a). We therefore conclude that certain impact prediction for 2036 can currently depend on the generally unmeasured masses of at least the first 29 additional perturbers.

*Integration error* Asteroid integrations normally use arithmetic truncated to 64-bits due to hardware limitations. Extended precision is possible using software algorithms that are ∼30 times slower and thus impractical for routine use. However, extended precision effectively eliminates the integration error growth found in normal 64-bit results. Therefore, we monitored the integration error when assessing asteroid perturbations by differencing 128- and 64-bit trajectory propagations. The 64-bit integrations used a maximum predictor/corrector order of 14/15 with a local error tolerance requirement of $10^{-14}$ (i.e., maximum difference between the method's numerical difference equation and the exact differential equation at an instant), while the 128-bit integrations used a maximum 21/22 order approach with a local error requirement of $10^{-19}$.

Although the 64-bit error accumulation was typically only a few hundred kilometers by 2036 (Table 6a), we found instances where the error was comparable to (or larger than) one Earth radius (Giorgini et al., 2005b). This occurred when the 64-bit algorithm was unable to meet the $10^{-14}$ local error tolerance and autonomously reduced the threshold to various values in

Table 6
Trajectory prediction error from 2006 to 2029 and 2036

(a) Planetary ephemeris, asteroids, integration error (Group 1):

| Model | Impacting trajectory | | | | Nominal (S142) trajectory | | | | Nominal (S142) trajectory | | | |
|---|---|---|---|---|---|---|---|---|---|---|---|---|
| | (fit-discontinuous) | | 64-bit error | | (fit-discontinuous) | | 64-bit error | | (fit-discontinuous) | | 64-bit error | |
| | 2029 km | 2036 km | 2029 km | 2036 km | 2029 km | 2036 km | 2029 km | 2036 km | 2029 km | 2036 km | 2029 km | 2036 km |
| 1. Planetary ephemeris | | | | | | | | | | | | |
| | −1.220 | +28,600 | | | −1.080 | +23,100 | | | +3.015 | −148,000 | | |
| 2. Asteroid perturbers | | | | | | | | | | | | |
| 128 | −0.354 | +14,700 | 0.011 | 441 | −0.364 | +15,200 | 0.358 | 14,300* | +0.163 | −5,400 | 0.017 | 688 |
| 64 | −0.336 | +13,900 | 0.015 | 581 | −0.377 | +15,700 | 0.002 | 76 | +0.192 | −6,830 | 0.004 | 182 |
| 32 | −0.307 | +12,600 | 0.013 | 493 | −0.365 | +15,000 | 0.005 | 186 | +0.109 | −3,700 | 0.063 | 2541* |
| 16 | −0.193 | +7,950 | 0.010 | 403 | −0.275 | +11,400 | 0.016 | 635 | +0.120 | −4,330 | 0.022 | 878 |
| 8 | −0.072 | +3,000 | 0.012 | 474 | −0.085 | +3,560 | 0.006 | 261 | +0.214 | −8,350 | 0.005 | 216 |
| 4 | −0.071 | +2,890 | 0.065 | 2590* | −0.054 | +2,200 | 0.022 | 890 | +0.102 | −4,000 | 0.005 | 195 |
| 3 | 0.000 | 0 | 0.051 | 2030* | 0.000 | 0 | 0.008 | 308 | 0.000 | 0 | 0.010 | 398 |
| 0 | +0.648 | −27,600 | 0.005 | 205 | +1.061 | −44,500 | 0.018 | 716 | +0.543 | −23,400 | 0.005 | 184 |

(b) Solar pressure and Yarkovsky (Group 2):

| Model type | Impacting trajectory (fit-discontinuous) | | Nominal trajectory (fit-discontinuous) | | Nominal trajectory (fit-continuous) | | | |
|---|---|---|---|---|---|---|---|---|
| | 2029 km | 2036 km | 2029 km | 2036 km | 2029 km | 2036 km | | |
| 3. Solar pressure | | | | | | | | |
| Minimum | −92 | +3,688,000 | −77 | +3,101,000 | −5.7 | +226,000 | | |
| Nominal | −138 | +5,565,000 | −117 | +4,673,000 | −8.5 | +360,000 | | |
| Maximum | −210 | +8,470,000 | −177 | +7,102,000 | −12.9 | +509,000 | | |
| 4. Thermal ("Yarkovsky") | | | | | Yarkovsky only | | Yarkovsky + Solar | |
| In-plane min. | +2.9 | −108,000 | +3.5 | −135,000 | +19.7 | −785,000 | +13.0 | −522,000 |
| max. | +5.8 | −220,000 | +7.4 | −285,000 | +40.4 | −1,610,000 | +26.0 | −1,040,000 |
| Prograde min. | −307 | +12,380,000 | −302 | +12,110,000 | −322 | +12,890,000 | −328 | +13,140,000 |
| max. | −703 | +28,320,000 | −692 | +27,660,000 | −741 | +29,550,000 | −755 | +30,120,000 |
| Retrograde min. | +286 | −11,600,000 | +285 | −11,440,000 | +325 | −13,040,000 | +318 | −12,770,000 |
| max. | +654 | −26,570,000 | +652 | −26,200,000 | +740 | −29,710,000 | +725 | −29,130,000 |

*Notes*. (a) Trajectory differences relative to the SDM caused by normally excluded factors. Initial heliocentric states were propagated using 128-bit (quadruple-precision) arithmetic from September 1, 2006 using $\mathrm{SDM}_{\mathrm{DE405}}$, then differenced with a propagation based on DE414 (line 1), then differenced with trajectories incorporating decreasing numbers of asteroid perturbers (line 2). Table values are for April 13.0 of 2029 and 2036, just prior to the encounters. Offsets are primarily in the along-track component. Negative and positive signs indicate delay or advance in arrival at the point of orbit intersection relative to the $\mathrm{SDM}_{\mathrm{DE405}}$ prediction. For the "Nominal (continuous)" case, the changed dynamical model was included in a re-estimation of the orbit solution using all data reported from 2004–2006. "64-bit error" columns are the integration error at each epoch for asteroid perturbation cases, determined by differencing the 128-bit trajectory with an otherwise identical 64-bit (double-precision) propagation. An asterisk ("∗") denotes cases for which a local error tolerance of $10^{-14}$ could not be maintained during the 64-bit integration producing larger errors. (b) For Group-2 parameters, impacting and nominal S142 trajectory differences relative to the SDM are shown for fit-discontinuous and fit-continuous accelerations due to reflection, absorption, and emission of radiation. For solar pressure (line 3), the minimum perturbation result is for the most massive, least reflective case ($d = 350$ m, $\rho_b = 3.1\ \mathrm{g\,cm^{-3}}$, and $p_v = 0.30$). The "nominal" case is a sphere with $d = 270$ m, $\rho_b = 2.7\ \mathrm{g\,cm^{-3}}$, and $p_v = 0.33$. The maximum perturbation is found for the least massive sphere with greatest reflectivity ($d = 210$ m, $\rho_b = 2.3\ \mathrm{g\,cm^{-3}}$, and $p_v = 0.35$). For Yarkovsky thermal re-radiation (line 4), "In-plane min." is the in-plane pole case having maximum mass and minimum absorption ($d = 350$ m, $\rho_b = 3.1\ \mathrm{g\,cm^{-3}}$, $p_v = 0.35$). "In-plane max." is the in-plane pole with minimum mass and maximum absorption ($d = 210$ m, $\rho_b = 2.3\ \mathrm{g\,cm^{-3}}$, $p_v = 0.30$). Prograde and retrograde cases are similarly denoted.

the $10^{-13}$ range. Inability to meet the error requirement can be due to planetary close-approaches, computational noise in the perturber models, or step-size and predictor–corrector order requirements. The 128-bit algorithm was always able to satisfy the tighter $10^{-19}$ local error requirement. We conclude that, if a local error of at least $10^{-14}$ can be maintained, 64-bit "double-precision" integration is sufficient to analyze even the impact trajectories. The much slower 128-bit "quadruple-precision" propagation is necessary only if the local error criterion cannot be met.

*Apophis encounters (144898) 2004 VD17* One Apophis encounter of potential interest is a nominal 6.71 LD approach to 2004 VD17 on July 17.9, 2034. 2004 VD17 is a PHA currently having a small estimated impact probability of $1.7 \times 10^{-8}$ in 2102. It was the 2nd object after Apophis to briefly be assigned a Torino Hazard Scale '2' (Morrison et al., 2004).

At the time of the encounter, Apophis' S142 $3\sigma$ uncertainty region extends ±51 million km along its orbit path, while 2004 VD17's $3\sigma$ uncertainty extends ±1800 km (solution #134). However, the two SDM statistical regions can come within

Table 7
Most significant asteroid perturbers during 2004–2036

| Rank | Asteroid | ∑PIN | H | STYP | $\rho$ (g cm$^{-2}$) | RAD (km) | ALB | GM (km$^3$ s$^{-2}$) | NCA | MinCA (AU) | AvgCA (AU) | Min$V_r$ (km s$^{-1}$) | Avg$V_r$ (km s$^{-1}$) | ∑PIN% | T_∑PIN% |
|---|---|---|---|---|---|---|---|---|---|---|---|---|---|---|---|
| 1 | 1 Ceres | 1621.1 | 3.3 | C | – | 476 | 0.09 | =63.2 | 16 | 1.48 | 1.66 | 6.19 | 10.28 | 43.23 | 43.23 |
| 2 | 4 Vesta | 713.0 | 3.2 | V | – | 265 | 0.42 | =17.8 | 25 | 1.22 | 1.45 | 6.27 | 12.09 | 19.02 | 62.25 |
| 3 | 2 Pallas | 150.9 | 4.1 | B | – | 266 | 0.16 | =14.3 | 11 | 1.03 | 1.51 | 7.91 | 13.92 | 4.02 | 66.27 |
| 4 | 10 Hygiea | 79.8 | 5.4 | C | – | 204 | 0.07 | =7.00 | 9 | 1.81 | 1.89 | 8.32 | 10.47 | 2.13 | 68.40 |
| 5 | 3 Juno | 53.1 | 5.3 | Sk | 2.7 | 117 | 0.24 | ∼1.21 | 14 | 0.94 | 1.49 | 2.97 | 11.30 | 1.42 | 69.82 |
| 6 | 16 Psyche | 52.1 | 5.9 | X | – | 127 | 0.12 | =4.49 | 13 | 1.32 | 1.74 | 5.21 | 12.38 | 1.39 | 71.21 |
| 7 | 15 Eunomia | 37.1 | 5.3 | S | 2.7 | 128 | 0.21 | ∼1.57 | 17 | 0.99 | 1.59 | 3.31 | 12.39 | 0.99 | 72.20 |
| 8 | 9 Metis | 33.6 | 6.3 | – | 2.7 | 95 | 0.12 | ∼0.65 | 26 | 0.89 | 1.50 | 4.32 | 12.67 | 0.90 | 73.09 |
| 9 | 7 Iris | 30.9 | 5.5 | S | 2.7 | 100 | 0.28 | ∼0.75 | 25 | 0.95 | 1.57 | 5.61 | 12.88 | 0.82 | 73.92 |
| 10 | 29 Amphitrite | 26.5 | 5.8 | S | 2.7 | 106 | 0.18 | ∼0.90 | 26 | 1.26 | 1.66 | 7.05 | 13.18 | 0.71 | 74.62 |
| 11 | 532 Herculina | 26.2 | 5.8 | S | 2.7 | 111 | 0.17 | ∼1.04 | 13 | 1.29 | 1.55 | 4.88 | 11.02 | 0.70 | 75.32 |
| 12 | 356 Liguria | 20.8 | 8.2 | – | 2.7 | 66 | 0.05 | ∼0.21 | 11 | 0.85 | 1.37 | 0.92 | 8.94 | 0.55 | 75.88 |
| 13 | 6 Hebe | 19.7 | 5.7 | S | 2.7 | 93 | 0.27 | ∼0.60 | 26 | 0.89 | 1.57 | 5.24 | 12.38 | 0.53 | 76.40 |
| 14 | 704 Interamnia | 19.6 | 5.9 | B | – | 158 | 0.07 | =5.00 | 7 | 1.54 | 1.80 | 7.47 | 13.13 | 0.52 | 76.92 |
| 15 | 52 Europa | 18.3 | 6.3 | C | 1.3 | 151 | 0.06 | ∼1.26 | 9 | 1.65 | 1.78 | 7.50 | 8.60 | 0.49 | 77.41 |
| 16 | 139 Juewa | 17.7 | 7.8 | X | 5.3 | 78 | 0.06 | ∼0.71 | 14 | 1.23 | 1.61 | 5.83 | 10.40 | 0.47 | 77.88 |
| 17 | 324 Bamberga | 17.1 | 6.8 | – | 2.7 | 115 | 0.06 | ∼1.14 | 15 | 1.01 | 1.50 | 9.09 | 12.48 | 0.45 | 78.34 |
| 18 | 20 Massalia | 15.1 | 6.5 | S | 2.7 | 73 | 0.21 | ∼0.29 | 26 | 1.02 | 1.59 | 4.24 | 13.61 | 0.40 | 78.74 |
| 19 | 14 Irene | 14.7 | 6.3 | S | 2.7 | 76 | 0.16 | ∼0.33 | 18 | 1.06 | 1.57 | 4.24 | 11.84 | 0.39 | 79.13 |
| 20 | 22 Kalliope | 14.5 | 6.5 | X | 5.3 | 91 | 0.14 | ∼1.10 | 13 | 1.68 | 1.80 | 7.51 | 11.58 | 0.39 | 79.52 |
| 21 | 511 Davida | 13.7 | 6.2 | C | 1.3 | 163 | 0.05 | ∼1.57 | 6 | 1.32 | 1.62 | 7.06 | 9.69 | 0.37 | 79.89 |
| 22 | 18 Melpomene | 13.4 | 6.5 | S | 2.7 | 70 | 0.22 | ∼0.26 | 25 | 0.79 | 1.42 | 2.83 | 11.60 | 0.36 | 80.24 |
| 23 | 69 Hesperia | 13.0 | 7.0 | X | 5.3 | 69 | 0.14 | ∼0.49 | 10 | 1.34 | 1.57 | 4.41 | 7.66 | 0.35 | 80.59 |
| 24 | 5 Astraea | 12.8 | 6.8 | S | 2.7 | 60 | 0.23 | ∼0.16 | 17 | 0.83 | 1.51 | 2.54 | 10.74 | 0.34 | 80.93 |
| 25 | 8 Flora | 12.6 | 6.5 | – | 2.7 | 68 | 0.24 | ∼0.24 | 24 | 0.93 | 1.31 | 4.23 | 11.38 | 0.34 | 81.27 |
| 26 | 19 Fortuna | 12.3 | 7.1 | Ch | 1.3 | 100 | 0.04 | ∼0.36 | 26 | 1.20 | 1.56 | 7.00 | 12.59 | 0.33 | 81.60 |
| 27 | 23 Thalia | 12.1 | 7.0 | S | 2.7 | 54 | 0.25 | ∼0.12 | 12 | 0.91 | 1.38 | 2.08 | 8.95 | 0.32 | 81.92 |
| 28 | 76 Freia | 11.5 | 7.9 | X | 5.3 | 92 | 0.04 | ∼1.15 | 5 | 1.62 | 1.81 | 5.29 | 6.98 | 0.31 | 82.23 |
| 29 | 45 Eugenia | 11.4 | 7.5 | C | 1.3 | 107 | 0.04 | ∼0.45 | 22 | 1.49 | 1.71 | 7.89 | 11.80 | 0.30 | 82.53 |
| 30 | 53 Kalypso | 11.4 | 8.8 | – | 2.7 | 58 | 0.04 | ∼0.15 | 16 | 0.82 | 1.48 | 1.82 | 10.32 | 0.30 | 82.84 |
| 31 | 712 Boliviana | 11.4 | 8.3 | X | 5.3 | 64 | 0.05 | ∼0.38 | 20 | 1.19 | 1.58 | 4.89 | 12.05 | 0.30 | 83.14 |
| 32 | 13 Egeria | 11.2 | 6.7 | Ch | 1.3 | 104 | 0.08 | ∼0.41 | 22 | 1.18 | 1.66 | 4.63 | 13.73 | 0.30 | 83.44 |

*Notes*. The orbit of each asteroid was numerically integrated to identify Apophis approach minima. "∑PIN" is the Perturbation Index Number of the object summed over all its encounters (Giorgini et al., 2002). It reflects the estimated total gravitational deflection of Apophis by 2036 due to that particular object and is the ranking basis. "H" is the measured absolute visual magnitude of the asteroid, "STYP" the observed spectral type, "$\rho$" the density assigned based on spectral type (2.7 g cm$^{-3}$, if STYP is unknown), "RAD" the radius. If RAD is unknown, it is computed from H and "ALB," the measured albedo of the object. "GM" is the asteroid's mass parameter. Measured GM values are preceded by an "=" symbol, while values inferred from H, RADI, or ALB are preceded by a "∼" symbol. "NCA" is the number of close-approach minima found. "MinCA" is the minimum close-approach distance, "AvgCA," the arithmetical mean close-approach distance. "Min$V_r$" is minimum relative velocity at encounter, "Avg$V_r$" the mean relative velocity. "∑PIN%" is the object's fraction of total summed perturbation for all objects, not just the 32 most significant shown. "T_∑PIN%" is the cumulative fraction of total perturbation from that and all other objects ranked higher in the list.

1.63 LD of each other at a point within 0.15$\sigma$ of the center of Apophis' uncertainty region.

This potentially raises questions as to the feasibility of redirecting one of the objects to impact the other, eliminating both Earth hazards simultaneously. Altering 2004 VD17's trajectory prior to its 0.021 AU Earth encounter on May 1.9 of 2032 (or Apophis' trajectory prior to the 2029 Earth encounter) in principle reduces energy requirements by leveraging a gravity assist to mutual impact in 2034. However, such an effort would still require the ability to impart a controlled velocity change to millions of tons of material such that the two objects simultaneously arrive within 100 m of the same predicted point in space years later. The measurement and prediction problems are substantial for such an approach and the analyses subsequently described herein illustrate its unreliability.

*3.1.2.3. Earth and Moon gravitational asphericity* To examine the point-mass assumption of the SDM, we represented the effect of the Earth's non-uniform mass distribution by a spherical harmonic expansion of its potential field (known as *EGM96*; Lemoine et al., 1998) and included it in the dynamical equations of motion.

The *EGM96* gravity model represents the Earth's potential field to degree and order 360 (360 × 360). It is based on the combined measurements of many satellites over many years. However, it is unlikely Apophis will be sensitive to the higher-order terms due to its short encounter times. Since there is significant computational overhead in evaluating the complete field's 130,317 coefficients at each integration step, we truncated the field to degree and order two (5 coefficients).

Comparing an integration spanning 2006–2036 to the prediction of the standard point-mass model, we found that even 2nd-order terms make no significant difference up to the 2029 encounter. However, the trajectories diverge thereafter, by 19,022 km in 2036 for the nominal trajectory. 99.5% of this error is in the negative along-track direction relative to the

Table 8
The decreasing effect of higher order zonal terms of Earth's gravity field on the Apophis nominal trajectory in 2036

| Order $J_{(2\to x,0)}$ | ΔSDM (km) | $\Delta J_{8,0}$ (km) | $\Delta J_{8,8}$ (km) |
|---|---|---|---|
| 2 | 18887.392 | 18.530 | −97.996 |
| 3 | 18870.118 | 1.256 | −115.270 |
| 4 | 18868.872 | 0.010 | −116.516 |
| 5 | 18868.873 | 0.011 | −116.515 |
| 6 | 18868.860 | −0.002 | −116.528 |
| 7 | 18868.861 | −0.001 | −116.527 |
| 8 | 18868.863 | 0.000 | −116.525 |

*Notes*. Column "ΔSDM" is the Euclidean metric of the heliocentric position vector predicted using a harmonic gravity model (complete to the order indicated by row) and the position vector predicted by the SDM point-mass model on 2036-April-13.0. The deviation is due almost entirely to the nearness of the single Earth encounter in 2029. Column "$\Delta J_{8,0}$" is the difference between a reference zonal model complete through $J_{8,0}$ and a zonal model complete only to the order indicated by its row, $J_{r,0}$. The decreasing differences with increasing order show decreasing sensitivity to a higher-resolution gravity model. Column "$\Delta J_{8,8}$" shows the position difference between a model complete to degree and order eight (not shown in table) and a zonal model complete only to the order indicated by its row, $J_{r,0}$ (an axially symmetric geopotential). The approach to a constant difference of approximately −116.5 km is the total extent to which the nominal prediction of the position of Apophis in 2036 is sensitive to longitudinal variations in the Earth's gravity field.

standard point-mass model. Therefore, an improved model of Earth's gravity field delays Apophis' predicted arrival at the intersection with Earth's orbit in 2036 relative to the SDM.

We increased the degree and order of the truncated field by one and repeated the process until reaching an 8th degree and order field (an "8 × 8" field) having 77 coefficient terms. The position differed from the point-mass prediction by 18,985 km (Fig. 6) and from the 7 × 7 field prediction by less than 2 m. The trend of decreasing trajectory difference with increasing order indicates little sensitivity to harmonic terms higher than 8th degree and order (8 × 8). A 4 × 4 field produces errors of less than 1 km by 2036 using 21 harmonic coefficients.

To determine if the gravity model could be simplified to include only the zonal harmonics of an axially symmetric Earth potential, we excluded tesseral and sectorial terms and increased order from 2 to 8. Inclusion of zonal terms to 4th order ($J_2$ through $J_4$) reduced trajectory sensitivity below 1 km (Table 8), but a bias of ∼116 km remained relative to the full 8 × 8 model. Therefore, the nominal Apophis trajectory has some sensitivity to the low degree and order longitudinal variations in Earth's potential field, but they are critical only for predicting a specific impact site.

We also examined consequences of a spherical harmonic lunar gravity model (*LP165P*; Konopliv et al., 2001). However, prior to 2036, Apophis comes no closer to the Moon than 55 lunar-radii and we find no significant trajectory difference from treating the Moon as a point-mass.

From this we conclude that the standard point-mass gravity model is insufficient to confirm an impact, producing more than $2.9R_\oplus$ of prediction error. Prior to 2029, Earth $J_2$ oblateness is the minimum gravity-field model required to produce errors less than one Earth-radius for any specific 2036 impact trajectory.

#### 3.1.2.4. Solar energy related perturbations

*Solar radiation pressure* Reflection of incident radiation at a surface causes a transfer of momentum to the body, producing a small, primarily radial acceleration in the heliocentric frame, included in our differential equations of motion as $d^2\boldsymbol{r}/dt^2 = (C_1 m^{-1}|\boldsymbol{r}|^{-2})\boldsymbol{F}$, where $\boldsymbol{r}$ is the Sun-to-body position vector, $t$ is time, $C_1$ is the solar flux at 1 AU (taken to be a constant $2.27545 \times 10^{-7}$ kg AU$^3$ m$^{-2}$ day$^{-2}$ although known to vary daily at the tenths of a percent level), and $m$ is the mass of the asteroid. $\boldsymbol{F}$ is a vector of geometric reflectivities: an illuminated half-sphere with a surface area scaled by a reflectivity factor of $(1 + S_p A)$, acting in the radial direction. $A$ is the Bond albedo and $S_p$ is a specular reflectivity coefficient, here taken to be unity. A slight drag due to relativistic aberration of momentum transfer in the heliocentric is a fraction of a percent of the total effect at Apophis' orbital speed and is not modeled. Surface albedo variations are considered later.

A recent paper by Rubincam (2007, Icarus, in press) considers the potential effect of north–south shape asymmetry on trajectory as a result of solar radiation. The analytic prediction for Apophis assumes extreme physical attributes (a symmetric flat-bottom half-sphere with no southern hemisphere) in combination with idealized attributes known to be invalid (no thermal inertia and 100% energy reflectance, although actual energy reflectance is less than 20%) to estimate a momentum transfer much greater than is possible for the real Apophis but less than other factors we studied. Therefore, the issue is not incorporated here.

In the IAU H-G two-parameter magnitude system (Bowell et al., 1989), the Bond albedo ($A$) is related to the measured geometric albedo ($p_v$), as $A = p_v \times q$ through the phase integral $q$, which numerically integrates to $q = 0.290 + 0.684 \times G$ ($0 \leqslant G \leqslant 1$). If the slope parameter $G$ is taken to be 0.25, a recommended value for moderate-albedo Sq class objects (Bowell et al., 1989), then $q$ for Apophis is ∼0.461.

The range of trajectory variation allowed by the unmeasured parameters of the solar pressure model is determined here by considering two extreme physical models still consistent with what is known. Each produces a minimum or maximum acceleration for a uniform albedo sphere consistent with Sq-class taxonomy, measured geometric albedo, and absolute magnitude ranges.

The maximum solar pressure acceleration exists for the smallest mass, most reflective possibility considered: a 210 m diameter object with bulk density ($\rho_b$) of 2.3 g cm$^{-3}$ and albedo of 0.35. The minimum solar pressure acceleration occurs with the largest mass, least reflective possibility: an object with $d = 350$ m, $\rho_b = 3.1$ g cm$^{-3}$, and $p_v = 0.30$. The "nominal" case is an object with $d = 270$ m, $\rho_b = 2.7$ g cm$^{-3}$, and $p_v = 0.33$. Masses considered therefore range from $1 \times 10^{10}$ to $7 \times 10^{10}$ kg. The dynamical equations of motion were augmented to include these three models and the measurement dataset refit to produce a new solution and predicted trajectory for each case.

Differencing both fit-continuous trajectories with the prediction of the SDM shows a position change in 2029 of be-

tween $[-12.9, -5.7]$ km, with a nominal offset of $-8.5$ km (Table 6b). The negative sign indicates a delay in arrival relative to the SDM prediction. By 2036, the position change is in the range $[+226{,}000, +509{,}000]$ km, with a nominal offset of $+360{,}000$ km.

Therefore, the SDM's exclusion of solar radiation pressure creates trajectory prediction errors comparable to a lunar distance by the time of the 2036 encounter. Even if solar pressure is included in the dynamics, uncertainties in the physical parameters of the asteroid (mass, albedo variation across the surface, shape, and solar flux variation) can cause trajectory variations spanning at least $44R_\oplus$.

*Thermal radiation acceleration* Momentum transfer to an asteroid may also be produced by time-delayed anisotropic thermal radiation, the consequences of which are referred to as the "Yarkovsky effect." This acceleration is a function of the asteroid's spin-vector, mass, optical and thermal properties, and shape. A diurnal component is produced by the longitudinal traverse of the sub-solar point as the body rotates, the heated surface subsequently radiating thermal photons. A seasonal component is caused by the change in insolation and emission aspect as the sub-solar point slowly shifts through a range of latitudes over an orbital period due to the asteroid's spin-pole obliquity.

Apophis' spin vector is the most significant unknown parameter and affects the direction and magnitude of the acceleration. We considered three extreme spin poles: prograde and retrograde spin around poles perpendicular to the orbit plane (which maximizes the diurnal component but eliminates the seasonal component) and a pole in the orbit plane (which maximizes the seasonal component but eliminates the diurnal component). For each case, we considered two variations: one with maximum absorptivity and minimum mass (maximizing the thermal acceleration) and one with minimum absorptivity and maximum mass (minimizing the thermal acceleration). These six cases are used to bound the magnitude of the Yarkovsky effect in an approach similar to what is described in Chesley (2006), but extended to the 2036 encounter based on the current best-estimate parameter set (primarily a smaller, less massive Apophis) and varying albedo instead of surface thermal conductivity.

Reasonable assumptions can be made for the other unmeasured parameters based on the available data. In addition to the size, bulk density, and albedo variations of the solar pressure model, polarimetric and infrared measurements suggest Apophis is unlikely to be bare rock, but has regolith to an unknown extent. Therefore, we consider a surface density of 1.7 $\mathrm{g\,cm^{-3}}$ and a surface thermal conductivity ($\kappa_0$) of 0.1 $\mathrm{W\,m^{-1}\,K^{-1}}$ (with $\kappa_0 = 1.0$ corresponding to bare chondritic rock and $\kappa_0 = 0.001$ thought to correspond to a highly porous surface) (Bottke et al., 2006). The equations of motion were extended to specify these six models, according to Vokrouhlický et al. (2000), using a linearized heat diffusion computational subroutine provided by Vokrouhlický and Chesley. We then refit the measurement dataset to produce a new solution and predicted trajectory for each case.

As summarized in Table 6b, the case least affected is the in-plane pole having minimum thermal absorption and maximum mass ($d = 350$ m, $\rho_b = 3.1$ $\mathrm{g\,cm^{-3}}$, $p_v = 0.35$). It produced a $+19.7$ km change in the along-track position by 2029 and a $-785{,}000$ km ($-123R_\oplus$) change by 2036. The largest perturbations occur for the prograde and retrograde poles perpendicular to the orbit plane having maximum thermal absorption and minimum mass ($d = 210$ m, $\rho_b = 2.3$ $\mathrm{g\,cm^{-3}}$, $p_v = 0.30$). Both cases produce position changes in the along-track direction of approximately 740 km by 2029 and 29,600,000 km ($4640R_\oplus$) by 2036, although in opposite directions.

We then combined solar pressure and the Yarkovsky models to assess the total effect of energy absorption, reflection, and emission (Fig. 7, Table 6b). The result is dominated by thermal radiation: for the two in-plane spin-vector cases, the Yarkovsky model contributes ∼65% of the combined effect, and for the four out-of-plane pole cases, it contributes ∼98%. The in-plane pole with minimum thermal absorption and maximum mass produces the least change: a $+13.0$ km advance in the along-track position by 2029 and $-522{,}000$ km ($-82R_\oplus$) delay by 2036. The maximum change relative to the SDM occurs for the prograde case with maximum thermal absorption and minimum mass: a $-755$ km delay in the along-track position by 2029 and a $+30{,}120{,}000$ km ($+4720R_\oplus$) advance by 2036. Radiative-energy forces change the location of the 2036 encounter prediction relative to the mapped covariance uncertainty region of SDM solution S142 by up to $\pm 1.4\sigma$.

*Trajectory alteration: Energy absorption and emission* Analysis of the dynamics of (29075) 1950 DA suggested the possibility of deflecting an object from impact by altering its absorption or emission properties, given hundreds of years to act (Giorgini et al., 2001; Milani, 2001; Ostro and Giorgini, 2004). For Apophis, despite the shorter time-scale, we find that radiative-energy forces can produce 82 to $4720R_\oplus$ of trajectory change by 2036, primarily due to amplification during the 2029 Earth encounter.

To assess the effectiveness of using this natural force to deflect Apophis, we consider a trajectory that impacts in 2036, varying energy absorption incrementally between ±5%, beginning on February 14, 2018. We then propagate the model forward using each of the six spin-vector cases of the combined solar pressure and thermal model. We found that changing total absorption or emission by 0.5% in 2018 created a trajectory shift greater than $R_\oplus$ by 2036 for all spin-vector and mass cases (Fig. 8).

The cases least sensitive to such change are the prograde and in-plane poles with minimum absorption and maximum mass: a 0.5% Bond albedo change still causes at least 6800 km ($1.1R_\oplus$) of along-track shift for both. The most responsive case is the retrograde pole with maximum absorption and minimum mass: a 0.5% Bond albedo change causes 48,000 km of shift ($7.5R_\oplus$).

This suggests that, if Apophis is on an impacting trajectory, altering the energy absorption and emission properties of a few hundred square meters of its surface (i.e., a $40 \times 40$ m patch) as late as 2018 could divert Apophis from impact in 2036;

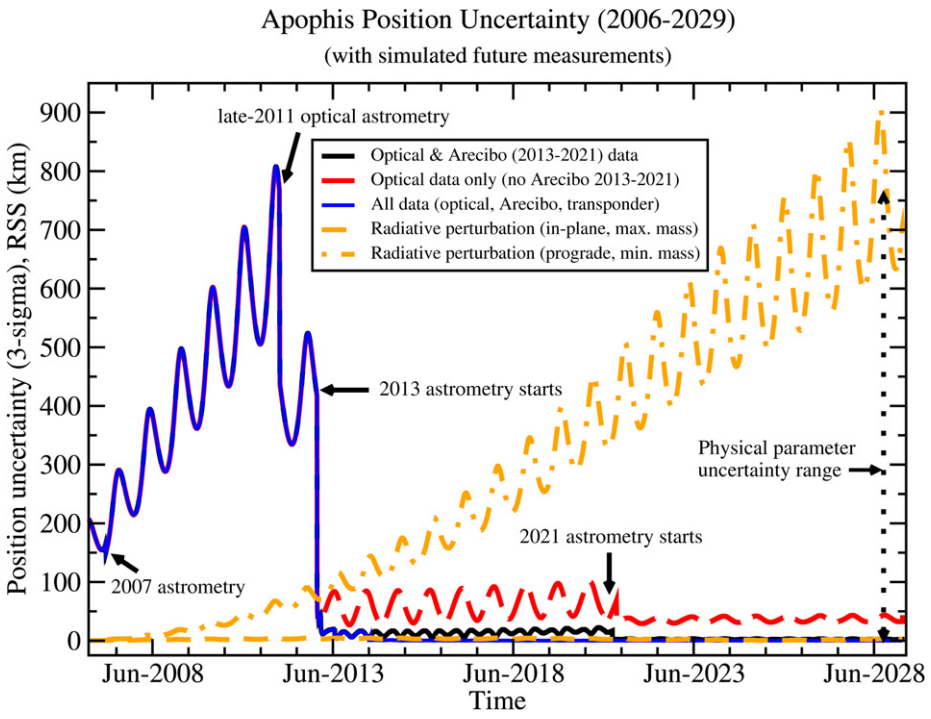


Fig. 7. Apophis instantaneous SDM $3\sigma$ formal position uncertainty during 2006–2029. The S142 solution covariance matrix was propagated using the SDM and a linearized, numerically integrated state transition matrix. Three different measurement simulations are shown beginning in 2013: optical only, optical with Arecibo in 2013 and 2021, and optical with Arecibo and transponder data. Also shown are the minimum and maximum radiation acceleration perturbation cases; the difference between the two curves is the position uncertainty due to the effect of solar energy. When radiative perturbation exceeds measurement uncertainty, it may be detectable depending on observation geometry.

that is, the currently unknown distribution of thermal properties across Apophis can make the difference between an impact and a miss.

Implementations of such a deflection might include depositing materials on Apophis' surface similar to the Kapton or carbon-fiber mesh sheets being considered for solar sails. With areal densities of 3 to 5 $\mathrm{g\,m^{-2}}$ (Garner, 2000; Whites and Knowles, 2001; Clark, 2000), 420 to 700 kg of carbon-fiber mesh could cover ~35–100% of the surface of Apophis in material with an emissivity of 0.4 to 0.9. For Kapton, static charge build-up in the material or asteroid due to solar UV exposure could aid deployment to the surface in such a low-gravity environment.

If an actionable hazard is found to exist, it would be necessary to move an object's entire uncertainty region (not just the nominal trajectory) away from the Earth. To provide margin adequate to cover all unknowns for Apophis, larger albedo modifications might be required. The modification required will therefore depend on the predicted size of the trajectory uncertainty region in 2036 and thus on the asteroid's physical properties.

### 3.2. Future measurements

To assess what measurements might exclude impact, indicate an actionable hazard, or detect perturbations from the SDM, we mapped the SDM solution covariance matrix to 2029 and 2036, beginning at epochs shortly after the most significant expected measurements in 2011, 2013, and 2021. We studied the effects of hypothetical 2-m ranging measurements in 2018, 2027, and 2029, such as from an in situ transponder.

Since the perturbations have an effect on the nominal trajectory similar to their effect on the impacting trajectory $-2.4\sigma$ distant in the uncertainty region (Tables 6a–6b), we separately compute the range of prediction uncertainty caused by the unmeasured physical properties of Apophis not in the SDM for the different solution dates. We add this parametric range to the SDM $3\sigma$ distribution extremes to provide calibrated position uncertainties for 2029 and 2036, along with criteria for excluding the potential impact without assigning probability distributions to the unmeasured parameters. Results are summarized in Table 9 and discussed below. This approach differs from the analysis in Chesley (2006), which develops a proxy Gaussian model for physical parameters related to thermal acceleration and assumes a spin-pole determination in 2013.

#### 3.2.1. 2007–2012

Potential optical measurements from early 2007 are included in the simulation as having 0.3 arcsec standard errors with respect to the nominal S142 trajectory. Apophis will subsequently remain close to the Sun in the sky at visual magnitudes 20.4–22.3, observable immediately before dawn or after twilight at low elevation angles. Optical astrometry will therefore be difficult to obtain during 2008–2010 (Fig. 9).

If optical astrometry is obtained during 2008–2010, the best ground-based measurements (~0.2 arcsec standard errors) cannot provide enough new information to significantly change the trajectory estimate until 2011–2012, other than to correct or cre-

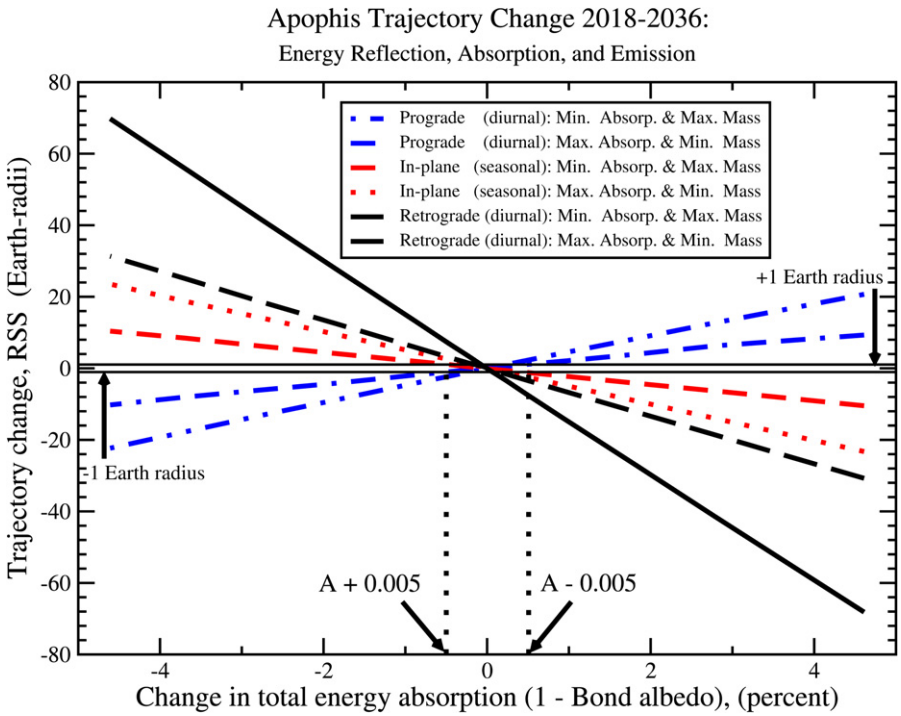


Fig. 8. Apophis deflection using albedo modification during 2018–2036. Thermal and solar radiation accelerations was modeled and the total energy absorbed altered by changing the Bond albedo ($A$). The resulting trajectory was differenced with the reference impact trajectory, for each of the six extreme spin-pole cases. A change of 0.5% in total absorption alters Apophis' position during the 2036 encounter by at least one Earth radius for all spin vector and mass cases considered.

ate systematic biases in the solution. This is because the plane-of-sky trajectory uncertainties are already less than 0.2 arcsec and comparable to reference star catalog errors (Fig. 9). However, such data could alter the covariance and thus SDM impact probability estimates.

When we include simulated 0.3 arcsec optical measurements from late 2011, the predicted SDM position uncertainty during the encounter of 2029 decreases 47%, from $\pm 1610$ to $\pm 860$ km ($3\sigma$). However, physical parameters not in the SDM create trajectory variations with an along-track interval extent of $[-570, 250]$ km at any point in the mapped SDM uncertainty region. Therefore, a more realistic "$3\sigma$" position uncertainty in 2029 is the interval sum $[-1430, 1110]$ km (Table 9). If impacting trajectories exist between $-1430$ and $-860$ km from the nominal center of the SDM distribution in the new solution, the SDM would tend to underestimate or discount the hazard, even if the dynamics still permit it. If impacting trajectories exist within $\sim$860 km of the center of the uncertainty region, the SDM would tend to over-estimate the impact probability by not reflecting the full range of uncertainties due to unmodeled physical parameters.

Extending to 2036 (Table 9), the calibrated along-track position uncertainties are $[-7030, 9040]R_\oplus$. If optical astrometry obtained in 2011 reduces uncertainties as expected, impact could be excluded without further physical characterization if the nominal SDM close-approach predicted for 2036 remains more than $+7030R_\oplus$ from Earth along the orbital track. The S142 estimated approach is already greater than this, at $+7890R_\oplus$. To encounter the Earth, Apophis would have to be located at less than $-3\sigma$ in the statistical covariance, be a retrograde rotator with a spin-pole nearly perpendicular to the orbit plane, and have less mass and greater absorptivity than the most extreme case considered here ($d = 210$ m, $\rho_b = 2.3$ g cm$^{-3}$, $p_v = 0.30$).

### *3.2.2. 2013*

During the 2013 Earth encounter, extensive radar measurements from Arecibo will be possible from February 11 to March 21 (0.5 and 1.0 μs delay and 0.1 Hz Doppler standard errors) and from June 13 to July 23 (1.0 μs delay and 0.1 Hz Doppler standard errors) with estimated SNRs of $\sim$40. Obtaining such Arecibo observations should enable direct size measurement, low-resolution three-dimensional shape reconstruction and spin-state estimation. This knowledge would collapse trajectory uncertainties produced by physical parameters. Accumulated radiation perturbation relative to SDM prediction will probably be detectable in Arecibo delay measurements unless Apophis is a high mass case with a near in-plane pole orientation (Fig. 7). Such cases may not be detectable from the ground until 2021 or later.

Our simulations show that Arecibo delay–Doppler measurements, combined with 0.3 arcsec optical astrometry, reduce the statistical position uncertainty mapped forward to 2029 by 97%, from $\pm 860$ to $\pm 22$ km ($3\sigma$). Given such data, the predicted 2029 along-track position uncertainty would be in the interval $[-550, 180]$ km, decreasing to a minimum of $\pm 22$ km, depending on what physical characteristics are determined and how precisely. This is denoted as $[-550, 180] \rightarrow \pm 22$ km, where the interval in brackets is a range without a defined probability distribution but $\pm 22$ specifies the $3\sigma$ bounds of a nom-

Table 9
Calibrated position uncertainties for Apophis

| Date | **2029** | | | **2036** | | |
|---|---|---|---|---|---|---|
| | $\pm 3\sigma$_Covar (km) | Param_model (km) | Calibrated (km) | $\pm 3\sigma$_Covar ($R_\oplus$) | Param_model ($R_\oplus$) | Calibrated ($R_\oplus$) |
| 2006 (Sep 01) | | | | | | |
| Solution S142 | 1610 | [−755, 724] | [−2370, 2330] | ∼10194.5 | [−4567, 4723] | ∼[−14800, 14900] |
| 2011 (Dec 31) | | | | | | |
| optical only | 855 | [−571, 251] | [−1430, 1110] | 5431.7 | [−1601, 3612] | [−7030, 9040] |
| 2013 (Aug 22) | | | | | | |
| optical only | 80 | [−528, 157] | [−610, 240] | 448.4 | [−1000, 3346] | [−1450, 3790] |
| (Arecibo, pole) | 22 | <[−528, 157] | <[−550, 180] | 150.4 | <[−1000, 3346] | <[−1150, 3500] |
| 2018: hypothetical s/c #1, Jan–Feb | | | | | | |
| 2-m ranging (Arecibo, pole) | 3 | <[−311, 57] | <[−310, 60] | 10.2 | <[−367, 1975] | <[−380, 1990] |
| 2021 (Jul 01) | | | | | | |
| optical only | 31 | [−198, −6] | [−230, 25] | 186.1 | [−32, 1255] | [−220, 1440] |
| (Arecibo, pole) | 2 | <[−198, −6] | <[−200, −4] | 10.1 | <[−32, 1255] | <[−40, 1270] |
| 2027: hypothetical s/c #2, Jan–Feb | | | | | | |
| 2-m ranging (Arecibo, pole) | 0.7 | <[−28, −6] | <[−29, −5] | 3.1 | <[40, 178] | <[40, 180] |
| 2029: radar, Jan–Feb | | | | | | |
| 2-m ranging (Arecibo,pole) | 0.6 | <[−0.9, −0.4] | <[−1.5, 0.2] | 2.4 | <[2.2, 5.1] | <[−0.2, 7.5] |

*Notes*. "$\pm 3\sigma$_Covar" columns are Apophis $3\sigma$ position uncertainties from linearized SDM covariance mappings that incorporate the astrometric measurements expected to be available at the end of the period of observability shown. "Param_model" shows the extreme positive and negative position offset produced by the dominant radiative perturbation models on the April 13 encounter dates in 2029 and 2036. "Calibrated" is the interval sum $[a, b] + \gamma[c, d] = [a + c, b + d]$, where $a = -3\sigma$, $b = +3\sigma$, $c =$ the most negative offset due to physical parameter models, $d =$ the most positive, and $\gamma$ is a scale factor. The sum approximately bounds position uncertainties due to SDM covariance statistics and unmeasured physical parameters. Here $\gamma = 1.0$, but could reasonably be ∼1.15 to allow for Apophis shape and $\kappa_0$ variations not modeled. Intervals preceded by a "<" symbol identify cases where physical characterization of Apophis beyond that of this study has occurred; e.g., a spin-pole or mass determination. In such a case, the calibrated uncertainty interval will be less, as $c$ and/or $d$ approach zero and the interval sum approaches the Gaussian $3\sigma$ range $[a, b]$, depending on what was determined and to what level of precision. Rows indicate the measurements added on that date for that row; "Arecibo, pole" indicates cases in which Arecibo astrometry is (or was) obtained in 2013, or physical characterization (e.g., pole determination) has previously occurred.

inally Gaussian measurement error model. By 2036, the along-track calibrated $3\sigma$ interval would be $[-1150, 3500]R_\oplus$ with no further physical characterization, or as little as $\pm 150R_\oplus$ with full characterization: $[-1150, 3500] \rightarrow \pm 150R_\oplus$ (Table 9). If the nominal Apophis close-approach in 2036, estimated using optical and Arecibo astrometry from 2013, is predicted to pass more than $1150R_\oplus$ ahead of the Earth, the impact hazard could be discounted without further physical characterization.

If there is no Arecibo radar experiment in 2013, range measurement, imaging, and shape inversion will not be possible; the predicted Goldstone radar SNR in 2012–2013 will be sufficient for 0.4 Hz Doppler measurements, but not for ranging. Such Doppler astrometry will not provide significant information; the predicted $3\sigma$ SDM uncertainties (RSS) mapped to the 2029 encounter are ∼ 78.5 km with Goldstone Doppler and ∼78.8 km without it. Uncertainty reduction would primarily come from the optical data; if Apophis is a low mass prograde (or retrograde) rotator, radiation perturbation might also be detectable in optical astrometry (Fig. 7). The calibrated along-track uncertainty interval would be [−610, 240] km by 2029 and $[-1450, 3790]R_\oplus$ by 2036 (Table 9). If the nominal close-approach is predicted to occur more than $1450R_\oplus$ ahead of the Earth in 2036, the impact hazard could be discounted without physical characterization or Arecibo astrometry.

A successful astrometry-only Arecibo experiment would reduce the calibrated position uncertainty interval 11% by 2036 compared to an optical-only apparition. However, if Apophis is physically characterized to a level beyond that of this study, the uncertainty reduction would be between 11% and 94% by 2036, depending on the extent of the characterization.

### 3.2.3. 2018 (hypothetical spacecraft mission 1)

If range measurements accurate to 2-m (from a transponder or spacecraft) are possible for several weeks in January–February of 2018, calibrated $3\sigma$ uncertainties predicted for 2036 would shrink to the interval $[-380, 1990] \rightarrow \pm 10.2R_\oplus$ (Table 9).

If deflection is considered, linear extrapolation of Fig. 8 reveals that modifying Apophis energy absorption or emission by 2–10% (worst-case, depending on spin, mass, and energy absorption) could produce a $6\sigma$ ($20.4R_\oplus$) trajectory change by 2036 and move the entire uncertainty region away from the Earth. Such a change might require less than 250 kg of material be distributed across the surface of Apophis.

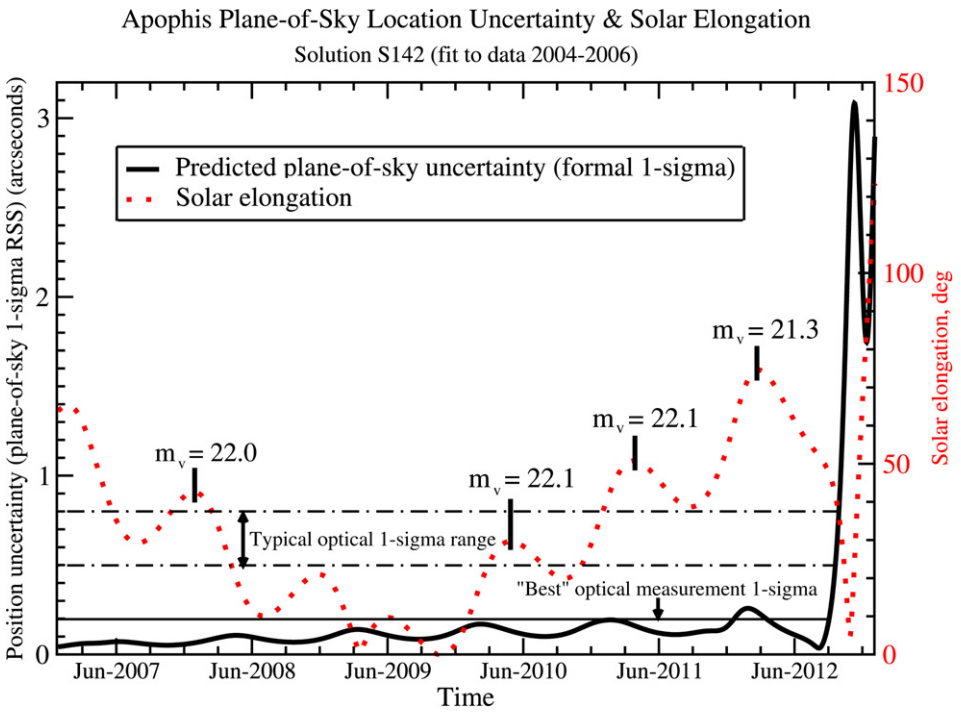


Fig. 9. Plane-of-sky position uncertainties during 2006–2013. The angular standard deviation of reference solution S142 is plotted with comparison lines showing "best" and "typical" ground-based optical astrometric measurement uncertainty. Solar elongation is plotted as a second curve using the scale on the right, with apparent visual magnitude ($m_v$) marked by vertical lines on key dates (e.g., times of maximum angular separation from the Sun). Measurement of such a dim object relative to background stars is problematic, particularly when less than 50° from the Sun in the sky.

However, if there is no further physical characterization of Apophis (beyond the parameters of this study), it will not be clear what deflection (if any) is necessary; a 30% change in absorption would be required to make a shift greater than the calibrated $3\sigma$ position uncertainty even for the most favorable retrograde case. If the pole is instead prograde or in-plane, absorption or reflection greater than 100% would be required; albedo modification could not provide a deflection significantly greater than the predicted uncertainties.

Therefore, if an actionable hazard remains after 2013, a follow-up spacecraft mission prior to 2021 would require physical characterization to assess whether deflection is necessary. Obtaining the information required to make the decision would simultaneously enable a solar energy deflection option that provides substantial performance margin.

### *3.2.4. 2021 (Earth close-approach)*

Arecibo SNRs >100 will be 3–4 times stronger than the 2013 apparition, sufficient for coarse resolution shape modeling. If Arecibo delay–Doppler measurements are obtained in 2021, the 2036 calibrated $3\sigma$ prediction uncertainty interval will be reduced to $[-40, 1270] \rightarrow \pm 10.1 R_\oplus$.

If no Arecibo radar data were obtained in 2013 and 2021, an optical-only dataset would have a calibrated uncertainty interval 1.3 to 82 times greater. The larger perturbation cases would remain optically detectable without radar (Fig. 7) and could constrain the position uncertainty within the interval $[-220, 1440] R_\oplus$.

If a new orbit solution based on optical astrometry obtained in 2021 predicts a nominal Apophis encounter more than $220 R_\oplus$ ahead of the Earth in 2036, impact could therefore be excluded without further physical characterization or radar astrometry in 2013 and 2021. If impact has not yet been excluded, a spacecraft mission might be required. Arecibo physical characterization could eliminate the need for such a mission by reducing calibrated $3\sigma$ uncertainties to near the $\pm 10.1 R_\oplus$ statistical minimum.

### *3.2.5. 2027 (hypothetical spacecraft mission 2)*

If range measurements accurate to 2-m (such as from a transponder) are possible for several weeks in January–February 2027, the calibrated $3\sigma$ interval becomes $[40, 180] \rightarrow \pm 3.1 R_\oplus$ by 2036. Trajectory prediction uncertainties at that time due to physical parameters are 12 to 60 times greater than those due to position measurement uncertainties (Table 9). Given physical characterization, geometric details of the SDM uncertainty region in target or impact plane coordinate systems could resolve the 2036 encounter circumstances and exclude impact.

If an impact hazard remains after Apophis' physical properties are known, modifying total absorptivity between 5% and 31% (depending on the properties) could produce a $6.2 R_\oplus$ trajectory change by 2036 and move the uncertainty region away from the Earth with a $6\sigma$ deflection.

### *3.2.6. 2029 (Earth encounter)*

If range measurements accurate to 2-m are possible for at least several weeks in January–February of 2029, the calibrated $3\sigma$ position uncertainty interval prediction for the April 2036 encounter becomes $[-0.2, 7.5] \rightarrow \pm 2.4 R_\oplus$ as of Febru-

ary 23 (Table 9). Absorptivity modification of 31–72% would be required to produce a minimal ($1R_\oplus$) trajectory change by 2036—insufficient change to reliably exceed position uncertainties at that time. Pole and shape changes several weeks later due to tides during the encounter could not alter Apophis' trajectory more than $1R_\oplus$ by 2036.

The current Arecibo and Goldstone radars would be able to detect and range Apophis from at least mid-February until after the encounter in mid-June in 2029. These measurements would finally provide certain impact assessment for 2036 if the possibility has not previously been excluded.

## 4. Conclusions

As the rate of asteroid discovery accelerates with new optical surveys, cases with persistently unresolved impact probabilities are likely to occur. Such initial hazard assessments will be based on measurement and dynamical models necessarily incomplete at some level.

For potentially hazardous cases preceded by a close planetary encounter, assessments based on the SDM may overestimate impact probability by excluding the effect of uncertain physical parameters, particularly for the more numerous sub-kilometer sized objects most strongly affected by solar energy. Conversely, when the SDM rules out a hazard, impact probability could be under-estimated for similar reasons. By reassessing the hazard of sub-kilometer objects given new measurements obtained in the years after a close planetary encounter, risks could be detected that otherwise would remain discounted. The minimum–maximum consequence of dynamical models can provide sufficient information to discount the threat or enable proper deflection decisions.

Small errors in the dynamical models are amplified by close encounters, making impact predictions across the encounter with the SDM problematic. However, such amplification offers the potential to redirect not only the object but its entire statistical uncertainty region away from Earth.

A deflection effort must be capable of producing a change in position substantially greater than the predicted position uncertainties at the time of the hazardous encounter. Those predicted uncertainties must include all significant parameters, not just those of the Standard Dynamical Model. Without such performance margin, the deflection action would instead create an unpredicted outcome or a new hazard.

## Acknowledgments

The authors thank Giovanni Valsecchi, an anonymous reviewer, Don Yeomans, and Paul Chodas for their review of the manuscript, and P. Chodas for generous use of his Monte Carlo software. Specific impact probabilities quoted are the values publicly posted by the JPL/Sentry system. We thank the technical staff at Arecibo Observatory for help with the observations. Part of this work was performed at the Jet Propulsion Laboratory (JPL), California Institute of Technology, under contract with the National Aeronautics and Space Administration (NASA). This material is based in part upon work supported by NASA under the Science Mission Directorate Research and Analysis Programs. The Arecibo Observatory is part of the National Astronomy and Ionosphere Center, which is operated by Cornell University under a cooperative agreement with the National Science Foundation.

## Appendix A. Estimation methodology and uncertainties

A valid prediction method should be self-correcting as new measurements are made and possess an error theory that describes the effect of error sources on the prediction.

A weighted least-squares estimate of orbital elements is self-correcting in that the sum of the squares of the weighted differences between each actual measurement and a predicted measurement (the "observed minus computed" residuals) is minimized by correcting the estimated position and velocity of the object (the state at an epoch) (Tapley et al., 2004; Crassidis and Junkins, 2004; Bierman, 1977; Lawson and Hanson, 1995).

The error model for the prediction begins with the assignment of measurement uncertainties. These uncertainties affect the state estimate, especially if the dataset is sparse or covers a short time period. Weights are formally the inverse of the measurement error variance ($1/s_w^2$), meaning measurements with greater specified variance have less influence in determining the correction applied to the original state. A zero-mean Gaussian measurement error model is assumed, and is usually closely realized for well-sampled datasets spanning an apparition or more. With proper assignment of measurement standard errors ($s_w$), a valid variance-covariance matrix for the estimated parameters results. This permits the linearized mapping of estimation error to other times of interest, as well as parameter sampling at the solution epoch.

Doppler measurements are generally assigned standard errors equal to one-fourth of the echo bandwidth. For coarse resolution ranging, delay measurements are generally assigned standard errors equal to the delay resolution or, if the echo is well-resolved in delay, one-half of the echo's delay depth. If an object's shape can be estimated, then the delay standard error is usually much smaller than the delay depth.

Optical measurement quality is more variable and usually depends on reporting site. The spherical angles Right Ascension (R.A.) and Declination (Dec.) at some instant are measured with respect to the known position of background stars in a reference catalog. Even at a particular observatory, measurement quality can vary from night to night depending on equipment, reduction method, star catalog, clock status, and observing conditions. There is rarely enough information to assign rigorous statistical variances. The measurement error model assumes R.A. and Dec. errors are uncorrelated, lacking specific information otherwise. Often, too few measurements are reported from a site to reliably characterize their variance or establish a Gaussian error model before measurement conditions change. This leads to the practice of treating optical angular data in a uniform way based on the Central Limit Theorem of probability theory. Standard errors have therefore historically been set

as 1.0 arcsec, based on general atmospheric seeing limitations and historical star catalog accuracies.

If groups of data from a particular observatory show evidence of systematic bias at a level near or greater than 1.0 arcsec relative to other reporting sites, the data may be de-weighted accordingly (or deleted, if clearly defective). However, if there is supporting information from a site, those measurements may be weighted more strongly if their fit-residuals support it, such as with the 0.3 arcsec and 0.5 arcsec data mentioned for Apophis.

Asteroid orbit solutions based on data from several sites spanning one or more apparitions tend to have a global residual quadratic mean (RMS) between 0.5 and 0.8 arcsec. This suggests that standard 1.0 arcsec uncertainties tend to underweight the optical data overall. However, historical results from several spacecraft encounters and more than 300 radar experiments have shown reliable predictive results using the standard weighting. The overall underweighting of optical data may compensate (if imperfectly) for uncalibrated or systematic biases that can occur when relating image measurements to an external coordinate system (such as $0.1''$ to $0.3''$ errors in reference star-catalogs).

## References


Behrend, R., Damerdji, Y., Reddy, V.V., Gary, B.L., Correia, H., 2005. (99942) 2004 MN4 combined light-curve. Available on-line at http://obswww.unige.ch/%7Ebehrend/r099942a.png.

Benner, L.A.M., Nolan, M.C., Giorgini, J.D., Chesley, S.R., Ostro, S.J., Scheeres, D.J., 2005. 2004 MN_4. IAU Circ. 8477.

Benner, L.A.M., Giorgini, J.D., Ostro, S.J., Nolan, M.C., Busch, M.W., 2006. (99942) Apophis. IAU Circ. 8711.

Bierman, G.J., 1977. Factorization Methods for Discrete Sequential Estimation. Academic Press, New York.

Bottke, W.F., Vokrouhlický, D., Rubincam, D.P., Nesvorny, D., 2006. The Yarkovsky and YORP effects: Implications for asteroid dynamics. Annu. Rev. Earth Planet. Sci. 34, 157–191.

Bowell, E., Hapke, B., Domingue, D., Lumme, K., Peltoniemi, J., Harris, A.W., 1989. Application of photometric models to asteroids. In: Binzel, R.P., Gehrels, T., Matthews, M.S. (Eds.), Asteroids II. Univ. of Arizona Press, Tucson, pp. 524–556.

Chesley, S.R., 2006. Potential impact detection for near-Earth asteroids: The case of 99942 Apophis (2004 MN4). In: Lazzaro, D., Ferraz-Mello, S., Fernández, J.A. (Eds.), Asteroids, Comets, Meteors: Proceedings of the 229th Symposium of the International Astronomical Union. Cambridge Univ. Press, Cambridge, pp. 215–228.

Clark, G. 2000. Breakthrough in solar sail technology. Available on-line at http://www.space.com/businesstechnology/technology/carbonsail_000302.html, March 20, 2000.

Crassidis, J.L., Junkins, J.L., 2004. Optimal Estimation of Dynamic Systems. Chapman & Hall/CRC Applied Mathematics & Non-linear Science, Boca Raton.

Delbò, M., Cellino, A., Tedesco, E.F., 2007. Albedo and size determination of (99942) Apophis from polarimetric observations. Icarus 188, 266–269.

Garner, C.E., 2000. Large area sail design concepts. In: IEEE Aerospace Conf. Proc., vol. 7, pp. 447–456.

Garradd, G.J., 2004. MPE Circ. 2004-Y25.

Giorgini, J.D., Chodas, P.W., Ostro, S.J., Benner, L.A.M., Hudson, R.S., Nolan, M.C., Margot, J.-L., Chamberlin, A.B., Chesley, S.R., Yeomans, D.K., 2001. Asteroid 1950 DA: Long term prediction of its Earth close approaches. In: Asteroids 2001: From Piazzi to the 3rd Millennium, Conference Abstracts, p. 205.

Giorgini, J.D., and 13 colleagues, 2002. Asteroid 1950 DA's encounter with Earth in 2880: Physical limits of collision probability prediction. Science 296, 132–136.

Giorgini, J.D., Benner, L.A.M., Nolan, M.C., Ostro, S.J., 2005a. Recent radar astrometry of Asteroid 2004 MN4. Bull. Am. Astron. Soc. 37, 521. Abstract.

Giorgini, J.D., Benner, L.A.M., Ostro, S.J., Nolan, M.C., Busch, M.W., 2005b. 99942 Apophis. IAU Circ. 8593.

Giorgini, J.D., Benner, L.A.M., Nolan, M.C., Ostro, S.J., 2005c. Radar astrometry of Asteroid 99942 (2004 MN4): Predicting the 2029 Earth encounter and beyond. Bull. Am. Astron. Soc. 37, 636. Abstract.

Konopliv, A.S., Asmar, S.W., Carranza, E., Sjogren, W.L., Yuan, D.N., 2001. Recent gravity models as a result of the lunar Prospector mission. Icarus 150, 1–18.

Krogh, F.T., 1968. A variable-step, variable-order multistep method for the numerical solution of ordinary differential equations. In: IFIP Congress, vol. 1, pp. 194–199.

Krogh, F.T., 1974. Changing stepsize in the integration of differential equations using modified divided differences. In: Bettis, D.G. (Ed.), Numerical Solution of Ordinary Differential Equations. In: Lecture Notes in Mathematics, vol. 362. Springer-Verlag, New York, pp. 22–71.

Larsen, J.A., Descour, A.S., 2004. MPE Circ. 2004-Y70.

Lawson, C.L., Hanson, R.J., 1995. Solving least squares problems. In: SIAM Classics in Applied Mathematics, vol. 15. Society for Industrial and Applied Mathematics, Philadelphia.

Lemoine, F.G., and 14 colleagues, 1998. The development of the joint NASA GSFC and NIMA geopotential model EGM96. NASA/TP-1998-206861, Greenbelt.

Milani, A., 2001. The sweet solution. In: Tumbling Stone, No. 5, Special Issue, Asteroids III Meeting, Santa Flavia, Palermo, Italy, 2001-June-15. On-line at http://spaceguard.esa.int/tumblingstone/issues/special-palermo/article1.htm.

Morrison, D., Chapman, C.R., Steel, D., Binzel, R.P., 2004. Impacts and the public: Communicating the nature of the impact hazard. In: Belton, J.S., Morgan, T.H., Samarasina, N.H., Yeomans, D.K. (Eds.), Mitigation of Hazardous Comets and Asteroids. Cambridge Univ. Press, Cambridge, pp. 353–390.

Moyer, T.D., 1971. Mathematical Formulation of the Double-Precision Orbit Determination Program (DPODP). JPL Tech. Report 32-1527.

Ostro, S.J., Giorgini, J.D., 2004. The role of radar in predicting and preventing asteroid and comet collisions with Earth. In: Belton, J.S., Morgan, T.H., Samarasina, N.H., Yeomans, D.K. (Eds.), Mitigation of Hazardous Comets and Asteroids. Cambridge Univ. Press, Cambridge, pp. 38–65.

Ostro, S.J., Hudson, R.S., Benner, L.A.M., Giorgini, J.D., Magri, C., Margot, J.-L., Nolan, M.C., 2002. Asteroid radar astronomy. In: Bottke, W.F., Cellino, A., Paolicchi, P., Binzel, R.P. (Eds.), Asteroids III. Univ. of Arizona Press, Tucson, pp. 151–169.

Scheeres, D.J., Benner, L.A.M., Ostro, S.J., Rossi, A., Marzari, F., Washabaugh, P., 2005. Abrupt alteration of the spin state of Asteroid 99942 Apophis (2004 MN4) during its 2029 Earth flyby. Icarus 178, 281–283.

Schweickart, R.L., 2005. A call for (considered) action. Presented at the National Space Society, International Space Development Conf., Washington, DC, May 20, 2005. On-line at http://www.b612foundation.org/papers/Call_for_Action.pdf.

Smalley, K.E., 2004. MPE Circ. 2004-Y25.

Standish, E.M., 1998. JPL Planetary and Lunar Ephemerides, DE405/LE405. JPL IOM 312.F-98-048, August 26, 1998.

Standish, E.M., 2006. JPL Planetary Ephemeris DE414. JPL IOM 343R-06-002, April 21, 2006.

Tapley, B.D., Schutz, B.E., Born, G.H., 2004. Statistical Orbit Determination. Elsevier, Boston.

Tucker, R., Tholen, D., Bernardi, F., 2004. MPS 109613.

Vokrouhlický, D., Milani, A., Chesley, S.R., 2000. Yarkovsky effect on small near-Earth asteroids: Mathematical formulation and examples. Icarus 148, 118–138.

Whites, K.W., Knowles, T.R., 2001. Calculating radiation force on carbon fiber gossamer space sailcraft. In: IEEE Antennas Propagat. Soc. Int. Symp. Dig., vol. 3, pp. 326–329.